https://doi.org/10.5194/egusphere-2026-288
Preprint. Discussion started: 10 February 2026

Review article:Advances in Polar Environmental Monitoring with ICESat-2: From Ice Sheet Mass Balance to Sea Ice Thickness Retrieval

Farui Jiang[1,2,3], Wenyu Shen[1,2,3],Chengen Wu[1,2,3], Yueyun Wang[1,2,3], Bing He[1,2,3], Zhongnan Yan[1,2,3], Xiaoping Pang[1,2,3*]

1 Chinese Antarctic Center of Surveying and Mapping, Wuhan University, Wuhan 430079, China.

2 Key Laboratory of Polar Environmental Monitoring and Public Governance, Ministry of Education (Wuhan University), Wuhan 430079,China

3 School of Geodesy and Geomatics,Wuhan University, Wuhan 430079,China

Corresponding author: Xiaoping Pang (pxp@whu.edu.cn)

129 Luoyu Road, Hongshan District, Wuhan, Hubei Province, China.

Abstract：

ICESat-2's advanced topographic laser altimeter system provides unprecedented technical support for polar environmental research including ice sheet mass balance detection and multi-dimensional sea ice parameter retrieval. However, the satellite's technical innovations and application advantages for polar environments still lack systematic elaboration, its high-precision data have not been effectively integrated from single-factor analysis to multi-process collaborative cognition, and the main sources of uncertainty as well as future technical breakthrough paths also remain unclear. To address these gaps, this review explores three core scientific questions. First, how to accurately solve the inversion challenges of key parameters through ICESat-2's technical innovations. Second, how to apply its high-precision inversion results to deepen the understanding of multi-sphere and multi-element interaction processes in polar regions and further reveal their systematic change laws. Third, what are the main uncertainties in ICESat-2's polar monitoring applications and what targeted technical paths can achieve breakthroughs. By systematically organizing relevant research progress, this review clarifies the inherent connection between technical innovations and polar parameter inversion, and ultimately provides solid support for the construction of cross-element integrated scientific cognition of polar environments.

Keywords: ICESat-2; Polar Environment; Sea Ice Thickness; Ice Sheet Mass Balance; Climate Change

https://doi.org/10.5194/egusphere-2026-288
Preprint. Discussion started: 10 February 2026

1 Introduction

As a core component of the global climate system, the cryosphere's dynamic changes are synergistically regulated by complex radiative and non-radiative interactions between the atmosphere, ocean, and ice (Goosse et al., 2018; Ding et al., 2021). Polar regions, as the central part of the cryosphere, have witnessed a series of significant changes in recent decades due to intensified global warming, including rapid Arctic sea ice shrinkage, accelerated Greenland Ice Sheet ablation, and permafrost degradation (Jahn et al, 2024; Michael et al., 2021; Liu et al., 2019; Qu et al., 2022). Acting as a key regulator of polar energy balance, sea ice has a surface albedo of 80%–90%, more than 10 times that of open oceans. Its retreat significantly enhances the ocean's capacity to absorb solar radiation, further amplifying polar warming (Serreze and Stroeve, 2015). Meanwhile, the massive freshwater stored in polar ice sheets, if fully melted, would cause a substantial rise in global sea levels, posing severe threats to coastal ecosystems and human societies (Pritchard et al., 2012). Therefore, accurately capturing changes in key polar environmental parameters and clarifying their systematic evolution laws are core prerequisites for understanding global climate change mechanisms and improving climate prediction capabilities.

Remote sensing serves as the primary means for large-scale, long-term polar monitoring, but traditional remote sensing technologies have inherent limitations in practice. ICESat-1's (Ice, Cloud, and land Elevation Satellite) single-beam observation design struggled to effectively distinguish slope effects from true elevation changes, leading to large errors in ice sheet mass balance inversion (Neuenschwander et al., 2008; Urban et al., 2005). CryoSat-2's radar signals are susceptible to snow penetration, significantly restricting the accuracy of sea ice thickness retrieval (Howat et al., 2008; Kwok et al., 2009). Launched in 2018, ICESat-2 with the advanced topographic laser altimeter system (ATLAS) overcomes traditional observational bottlenecks via revolutionary photon-counting technology, elevating key cryospheric parameter monitoring accuracy to the centimeter level and providing a novel technical approach for precise cryospheric monitoring (Markus et al., 2017).

Despite the breakthroughs brought by ICESat-2 to cryosphere research, a systematic review of existing studies reveals several key scientific gaps and weaknesses. Specifically, while technical parameters such as the six-beam spatial distribution of the ATLAS system have been explicitly disclosed, and related studies have developed algorithms based on these technical characteristics and verified their accuracy improvement effects (Liu et al., 2022), most of these studies merely present inversion results without systematically elaborating on ICESat-2's technical design and application advantages for polar environmental observations.

Secondly, existing research mainly focuses on single-factor or local-scale observational analyses, such as ice sheet mass balance (Brunt et al., 2021), ice shelf stability analysis (Li et al., 2020; Li et al., 2022), lead detection (Petty et al., 2021), and sea ice thickness changes. It fails to integrate the aforementioned high-precision observational data to deepen the scientific understanding of multi-sphere and multi-factor interaction processes in polar regions, thereby revealing the systematic change laws of the polar environment. Finally, although dominant uncertainties in ICESat-2's cryosphere observations have been initially identified and targeted resolved (Petty et al., 2023; Kwok et al., 2021), core uncertainties such as snow depth estimation biases, complex terrain observation interference, and inherent limitations of the observation system lack systematic classification and in-depth analysis of their combined

https://doi.org/10.5194/egusphere-2026-288
Preprint. Discussion started: 10 February 2026

impact mechanisms. This restricts the reliability verification of ICESat-2's observational results and forms a bottleneck for the technological development of the next generation of laser altimetry satellites.

To address the above scientific gaps, this review will systematically explore three aspects: (1) By systematically reviewing ICESat-2's core technical innovations, multi-level data product system, and adaptive design for extreme polar environments, deeply elaborate on its technical mechanisms for solving inversion challenges of key polar environmental parameters such as ice sheet mass balance and sea ice thickness. (2) By systematically integrating the understanding of polar ice sheet/ice shelf stability and multi-dimensional sea ice parameter retrieval from ICESat-2, construct a holistic scientific cognition of the systematic change laws of the polar environment. (3) By systematically clarifying the resolution of dominant observational uncertainties by ICESat-2 and the main remaining uncertainty sources, deeply analyze the impact mechanisms of each source, and further clarify feasible technical paths for targeted breakthroughs in the future. Notably, although ICESat-2 has also demonstrated significant value in ecological fields such as large-scale biomass estimation and global carbon stock assessment (Lefsky et al., 2005; Neumann et al., 2019; Yu et al., 2024; Zhu et al., 2020), to maintain the focus of the research theme, this review will only systematically summarize its progress in cryosphere science, with a particular emphasis on polar environments.

2 ICESat-2/ATLAS Observation System and Its Mechanistic Link to Polar Environmental Parameter Retrieval

The core technical innovations of ATLAS provide basic support for the retrieval of key polar parameters by establishing high-precision and high-density observational capabilities; the multi-level data product system realizes the effective conversion of raw observational data into key polar environmental parameters through targeted preprocessing and refined processing procedures; the adaptive design of the observation system for polar environmental characteristics ensures the reliability and stability of the retrieval process in different scenarios. The integration of these three aspects enables ICESat-2 to significantly improve the accuracy and applicability of polar environmental parameter retrieval.

2.1 Historical Evolution of Technical Innovations in the ICESat Series

In cryospheric change research, the ICESat mission launched by NASA in 2003 has provided crucial observational data. Through laser altimetry technology, the satellite played a central role in assessing the mass balance of mountain glaciers and polar ice sheets (Gardner et al., 2011; Urban et al., 2008). Based on its elevation data, researchers first achieved spatialized estimates of the mass balance of glaciers in the Hindu Kush–Karakoram–Himalaya region (Kääb et al., 2012), global peripheral glaciers, and the Greenland Ice Sheet (Bolch et al., 2013). Additionally, ICESat was successfully applied to the remote sensing retrieval of sea ice freeboard, thickness, and volume (Farrell et al., 2009; Connor et al., 2013). However, despite its remarkable achievements, ICESat's single-beam observation mode had obvious limitations in analyzing complex cryospheric processes: particularly in regions with rugged terrain, the sensor struggled to effectively distinguish slope effects from true elevation changes, requiring multi-period observational data for signal separation (Moholdt et al., 2010; Abdalati et al., 2010). Meanwhile, the low spatial resolution of the single beam limited its ability to capture microfeatures such as sea ice cracks and melt

https://doi.org/10.5194/egusphere-2026-288
Preprint. Discussion started: 10 February 2026

ponds, restricting the accuracy of sea ice type identification and thickness retrieval. Coupled with laser lifespan issues, its scientific data collection ceased in 2009.

Building on this, NASA launched the next-generation ICESat-2 satellite on September 15, 2018, which officially initiated scientific observation missions on October 14 of the same year. Compared with the previous mission, ICESat-2 effectively addressed the limitations of ICESat's single beam in spatial resolution and terrain slope measurement by equipping the ATLAS and a six-beam observation configuration (Howat et al., 2008), significantly enhancing the high-precision monitoring capabilities for glaciers, ice sheets, and sea ice (Magruder et al., 2020). Its observational technical characteristics are reflected in three core dimensions: observational geometry design, detection technology innovation, and positioning/coverage accuracy (**Figure 1**).

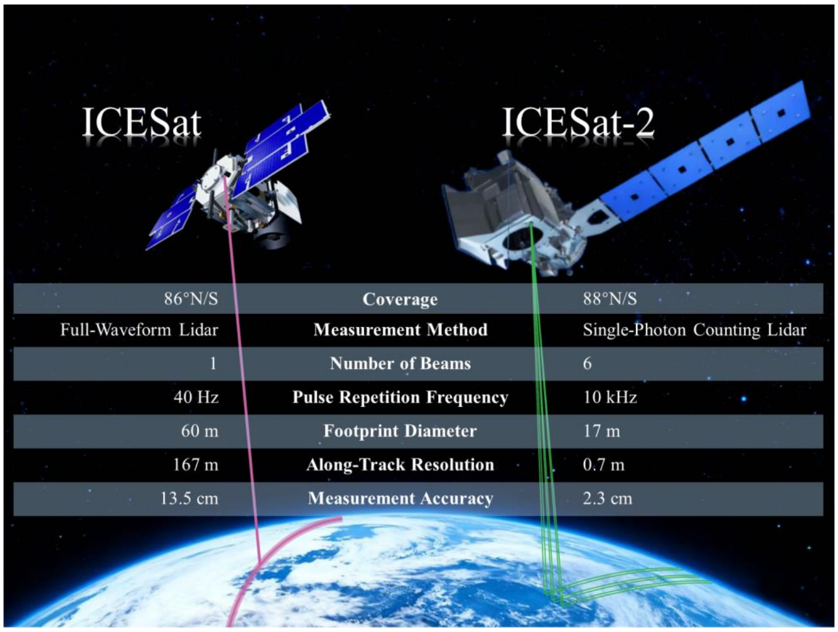

Figure 1. Schematic diagrams of the satellite sampling configurations for ICESat and ICESat-2

In terms of observational geometry design, the ATLAS altimeter onboard ICESat-2 constructs a high-density 3D observation network through an innovative configuration of three pairs of beams and yaw angle optimizatio, whose core technical design logic can be summarized as multi-beam collaborative coverage and dynamic energy adaptation. Specifically, unlike the first-generation ICESat's single-beam along-track sampling mode, ATLAS splits a single laser beam into three pairs of left, nadir, and right beams using diffractive optical elements. Combined with a 2° yaw angle design, the strong and weak energy beams within the same beam pair form a cross-track spacing of approximately 90 meters. Ultimately, the six ground tracks have an along-track spacing of about 3 kilometers and a total cross-track width of approximately 6 kilometers, achieving a systematic expansion of the observational coverage (Neumann et al., 2019) (**Figure 2**). Meanwhile, the system adopts a parameter combination of 0.7-meter along-track sampling interval and 11-meter laser footprint diameter to enhance the ability to capture microtopographic features; the 4:1 energy ratio design of strong and weak beams forms a differentiated adaptation mode for different surface reflectivity

https://doi.org/10.5194/egusphere-2026-288
Preprint. Discussion started: 10 February 2026

characteristics—high-energy strong beams meet the signal capture needs of low-reflectivity regions, while low-energy weak beams effectively avoid signal saturation in high-reflectivity regions (Kwok et al., 2022).

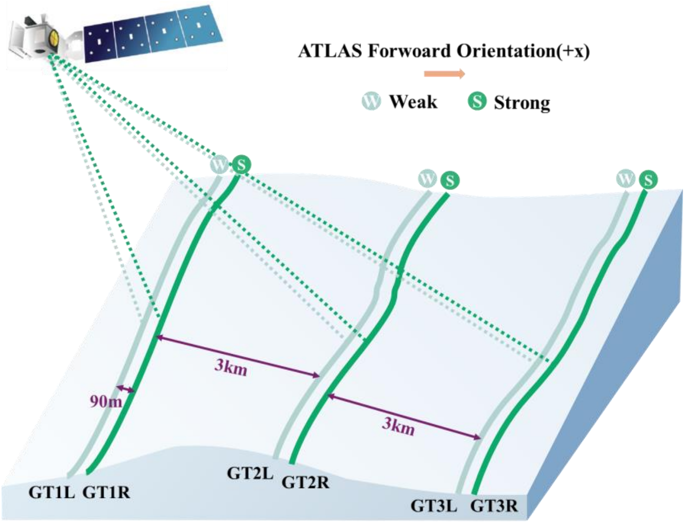

Figure 2. The ICESat-2 observational geometry: multi-beam configuration, laser footprints, and ground tracks.

In terms of detection technology innovation, ATLAS's photon-counting lidar technology breaks through the limitations of traditional pulse waveform detection, enabling accurate capture of weak signals. Unlike the first-generation ICESat, which obtained elevation information by integrating pulse echo waveforms, ATLAS can record the position and time of each returning single photon from laser pulses, constructing a high-resolution 3D photon cloud (Kwok et al., 2021). This technical characteristic endows the system with extremely high sensitivity to single-photon signals, enabling effective discrimination of different surface types in mixed high- and low-reflectivity regions. Additionally, the high temporal resolution of photon-counting technology, combined with multi-source data fusion from GPS receivers, star trackers, and the Laser Reference System (LRS), achieves centimeter-level 3D geolocation accuracy (Magruder et al., 2020).

In terms of positioning and coverage capabilities, ATLAS adopts a near-polar orbit design (inclination of 92°, covering 88°S to 88°N) combined with the uniform distribution of 1387 independent Reference Ground Tracks (RGTs), achieving comprehensive coverage of key global regions and addressing the insufficient coverage of the first-generation ICESat in polar marginal areas (Abdalati et al., 2010). The system sets an average operating altitude of 496 kilometers and a revisit period of 91 days, balancing observational efficiency and spatiotemporal resolution; it not only enables temporal dynamic monitoring of target parameters but also ensures the spatial representativeness of regional-scale observations through uniform track distribution (Markus et al., 2017).

2.2 Multi-Level Data Product System of ICESat-2

ICESat-2 has constructed a multi-level data product system from Level-1 to Level-3, which realizes the effective conversion of raw photon data into retrieval parameters through targeted preprocessing and refined processing procedures, serving as a core bridge connecting the observation system and parameter retrieval (Magruder et al.,

https://doi.org/10.5194/egusphere-2026-288
Preprint. Discussion started: 10 February 2026

2020) (**Figure 3**). Through a hierarchical processing logic to accurately address the retrieval needs of different scenarios, this product system forms a close mechanistic link with polar environmental parameter retrieval: Level-1 products achieve initial calibration of raw observational data, providing a high-quality foundation for subsequent processing; Level-2 products extract reliable surface elevation information through purification and screening of photon-level data; Level-3 products conduct dedicated refined processing and parameter retrieval for the retrieval needs of different polar environmental parameters, ultimately forming thematic products adapted to different retrieval objectives (Kwok et al., 2023).

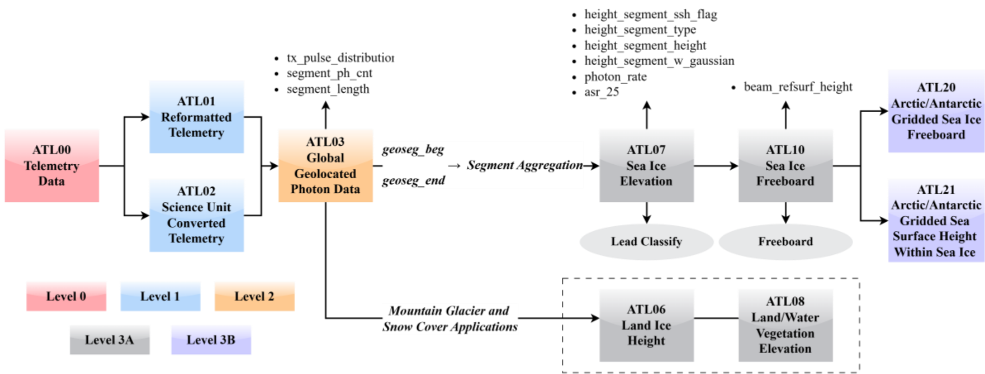

Figure 3. Overview of the ICESat-2 ATL data product suite and their hierarchical relationships

The processing flow from Level-1 to Level-2 products focuses on addressing the fundamental challenge of raw photon data purification and elevation extraction, thereby providing a unified, high-quality elevation dataset for all cryospheric parameter retrievals. Level-1 products, including ATL01 (raw time tags and photon response counts) and ATL02 (geophysical range correction), achieve the initial standardization of raw observational data through instrument temperature and voltage effect correction, as well as geophysical range calculation—effectively eliminating systematic errors inherent to the instrument itself (Kwok et al., 2020b).

Building on this, Level-2 product ATL03 provides high-precision 3D coordinates for each photon through solid tide, polar tide, ocean loading tide and total atmospheric delay correction, constructing a raw photon cloud dataset (Kwok et al., 2020a; Xie et al., 2023). The preprocessing flow of ATL03 including photon aggregation, surface detection, noise removal and scattering correction directly serves the goal of reliable surface elevation extraction. Initial separation of signal photons and background noise is achieved through continuous pulse photon clustering and height histogram construction. Outlier photons are removed using local mode positioning and window truncation methods, effectively suppressing the impact of background noise and first-photon bias. Elevation data accuracy is optimized through subsurface scattering correction, ultimately converting raw photon cloud data into clean and precise surface elevation data to provide core foundational support for subsequent cryospheric parameter retrieval.

Among Level-3 thematic products, ATL07 and ATL10 are the core backbone products for sea ice research. Together with ATL20/21, they form a sea ice parameter retrieval chain from core parameter retrieval to macro-scale integration, realizing accurate conversion from elevation data to sea ice freeboard. As the basic core product for sea

https://doi.org/10.5194/egusphere-2026-288
Preprint. Discussion started: 10 February 2026

ice parameter retrieval, ATL07 takes the purified elevation data from ATL03 as input. After a series of geophysical corrections based on the CryoSat-2 and DTU13 mean sea surface models, GOT4.8 tide model, and GEOS-FP-IT atmospheric inverse pressure correction (**Andersen et al., 2015**), it generates height segments by aggregating 150 consecutive signal photons, with segment intervals automatically adjusted based on photon density and surface reflectivity (**Kwok et al., 2019; Kwok et al., 2020b**). It adopts a decision tree classification algorithm based on three core parameters—surface photon rate, photon distribution width, and background noise rate (**Kwok et al., 2023**)—which can accurately distinguish surface types such as sea ice, open water, and clouds, while providing geographic location, observation time, and confidence information, laying a solid data foundation for subsequent ATL10 freeboard retrieval (**Table 1**).

Table 1 Detailed definitions of relevant fields in the ATL07 product

Field Type	Field Name	Unit	Field Description
classification features	height_segment_asr_calc	/	calculated apparent surface reflectivity
	height_segment_height	m	segment surface height
	height_segment_w_gaussian	m	best-fit Gaussian width
	height_segment_length_seg	m	segment length
	n_pulse_seg_used	m	the number of photons used in each height segment
	photon density	/	calculated by dividing the number of photons used by the length of the height segment
	photon_rate	photon	photon rate
	hist_w	m	width of photon height distribution
	background_r_norm	Hz	normalized background rate (50 pulses)
original classification	height_segment_ssh_flag	/	sea ice classification (0 = sea ice; 1 = sea surface)
	height_segment_type	/	segment surface type
quality control	fit_quality_flag	/	(-1 = invalid; 1 = optimal)
	n_pulse_seg_used	/	number of laser pulses used in sea ice segments
	height_segment_quality	/	height segment quality flag
cloud	cloud_flag_asr	/	cloud probability flag based on apparent reflectivity

ATL10 is the core dataset for ICESat-2 sea ice research, directly conducting sea ice freeboard estimation based on ATL07 classification results: it constructs a local sea surface reference by identifying valid sea surface height segments and calculates the freeboard difference of sea ice height segments relative to this reference. To improve statistical robustness, ATL10 adopts an adaptive aggregation design with an approximately 10-kilometer neighborhood window to generate freeboard scan segments; the window length and sampling interval can be dynamically adjusted according to sea ice distribution density, and no scan segments are generated for tracks lacking reliable sea surface references to avoid additional uncertainty. Each scan segment is accompanied by uncertainty assessment and quality indicators integrating factors such as beam quality and distance from the sea surface reference, while providing a freeboard histogram constructed from full-beam data to characterize the freeboard distribution within the scan segment (**Kwok et al., 2019**). As an extension of ATL10, the ATL20/21 gridded products map along-track freeboard and sea surface height data to a 25-kilometer polar stereographic projection grid, generating daily/monthly scale sea ice freeboard statistics and monthly scale sea surface height information (**Kwok et al., 2021**), realizing scale upgrading from fine observations to regional-scale and long-term sea ice research and providing support for macro cryospheric system change analysis.

https://doi.org/10.5194/egusphere-2026-288
Preprint. Discussion started: 10 February 2026

In addition, to meet the retrieval needs of ice sheets and mountain glaciers, the ATL06 product provides high-precision surface elevation through linear segment fitting, adapting to the need for accurate capture of elevation temporal changes in the retrieval of parameters such as ice sheet mass balance and glacier retreat rate; its extension to non-glacial mountainous areas also provides supplementary support for snow depth retrieval and topographic mapping (**Smith et al., 2019; Deschamps-Berger et al., 2023**). Based on photon classification, the ATL08 product provides both surface and vegetation height information over longer linear segments, primarily serving forest structure and biomass assessment (**Neuenschwander et al., 2021**).

2.3 Adaptive Design of ICESat-2 for Polar Environments

Polar environments exhibit significant spatiotemporal heterogeneity. Core characteristics such as surface reflectivity differences, seasonal dynamic evolution, and polar solar radiation interference directly affect the quality of laser observational signals and the reliability of retrieval results. The core advantage of the ICESat-2 observation system lies in forming targeted environmental adaptation mechanisms through technical innovations. Through the collaborative optimization of observational strategies and data processing flows, it effectively offsets the interference caused by environmental heterogeneity, ensuring the stability and accuracy of parameter retrieval in different scenarios.

The first core environmental challenge is the extreme heterogeneity of surface reflectivity. Different surface cover types in polar environments form a strong contrast pattern of "high reflectivity—low reflectivity": the reflectivity of snow-covered sea ice, snow cover, and other regions can reach 0.7–0.8, while that of leads, dark cracks, and other regions is only 0.1–0.2, a difference of nearly an order of magnitude (**Kwok et al., 2021b**). This contrast risks signal saturation in high-reflectivity areas and noise-induced signal loss in low-reflectivity regions, limiting capture efficiency (**Kwok et al., 2022**) (**Figure 4**). The ATLAS system addresses this through differentiated energy output of strong and weak beams, matching reflectivity-specific signal needs to avoid saturation or insufficient capture, and high-density multi-beam distribution that ensures complete coverage of heterogeneous surfaces without observational blind spots.

The second core environmental challenge is the dynamic interference of polar solar radiation. ATLAS's 532 nm visible band is vulnerable to solar background noise, with polar day-night alternation and varying solar elevation angles amplifying interference complexity (**Kwok et al., 2020a**). Background photon counts exceed signal photons by multiple times when solar elevation exceeds 30°, drowning effective signals, while interference is negligible below 10° or during polar nights—this dynamic directly impacts signal-noise distinction accuracy (**Kwok et al., 2019; Liu et al., 2024**). ICESat-2 mitigates this by scheduling core polar observations during twilight or nighttime to avoid high solar angles, and integrating solar elevation angle into signal screening algorithms with dynamic noise thresholds. High solar angles trigger strengthened verification of surface photon rate and background noise rate linear relationships to remove abnormal photons; low angles shield uncertain background noise parameters, extracting signals solely via spatial distribution characteristics (**Kwok et al., 2023**).

The third core environmental challenge is the seasonal dynamic evolution of polar environments. Polar environments exhibit region-specific seasonal changes: Arctic sea ice develops melt ponds and ablates marginally in summer, while thickening and forming cracks in winter; Antarctic Ice Sheet margins see accelerated ice shelf calving and ablation in summer, with snow accumulation and smooth surfaces in winter (**You et al., 2021; Shen et al., 2021**).

https://doi.org/10.5194/egusphere-2026-288
Preprint. Discussion started: 10 February 2026

These differences reduce the accuracy of fixed retrieval algorithms. ICESat-2's data product system addresses this through dynamically adaptive classification algorithms in core sea ice products ATL07 and ATL10. A refined classification system distinguishes clouds, sea ice, and crack types like specular, dark, and rough during the growth season (October–May) to match winter sea ice structure retrieval needs (Kwok et al., 2023). The system simplifies to clouds, sea ice/melt pond mixtures, and cracks/melt ponds during the ablation season (June–September), focusing on core surface types to ensure basic retrieval requirements.

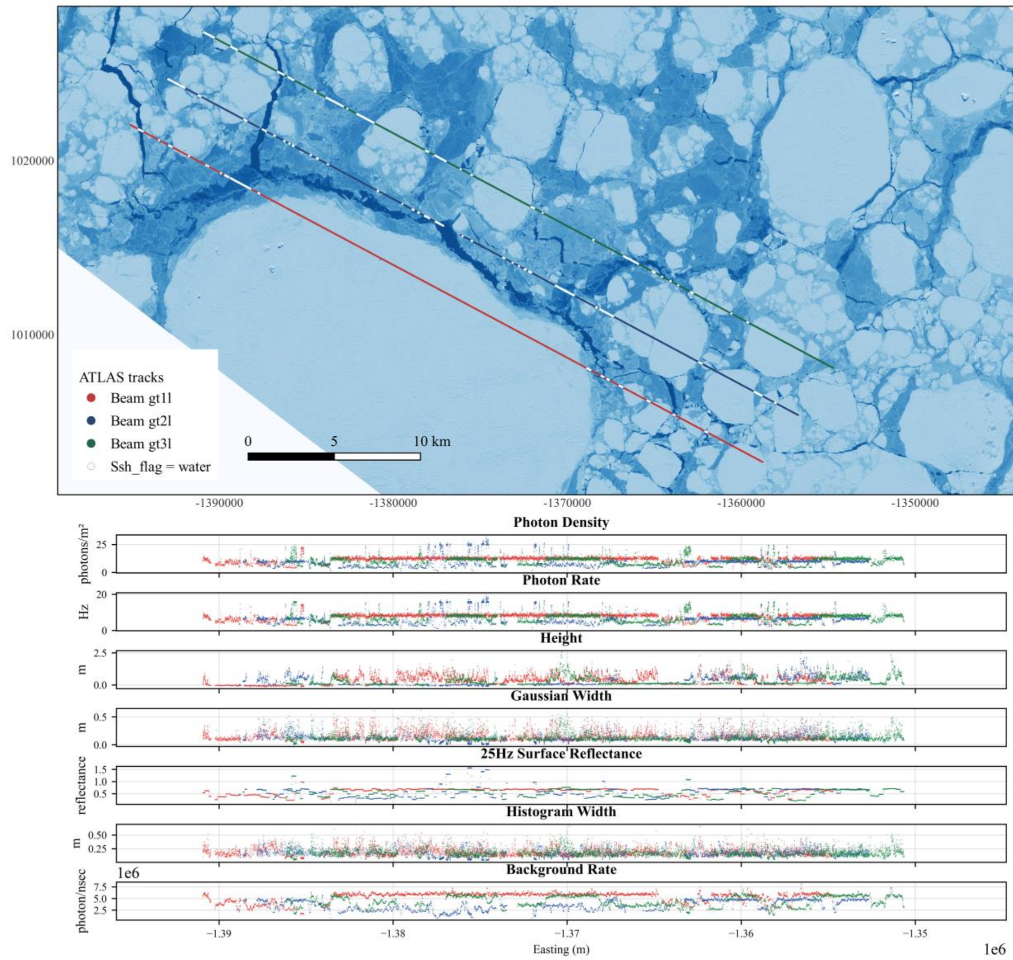

Figure 4. The main figure uses a S2 image as the background, with the laser altimetry ground tracks of the strong beams (gt1l, gt2l, gt3l) from the ATL07 product overlaid. The white areas in the figure represent the sea surface range identified by the ATL07 product. The series of subfigures respectively show the reflection characteristics of key parameters in the ATL07 product, including photon density, photon rate and other parameters.

3 ICESat-2 Observation Results Support In-depth Understanding of the Systematic Change Laws of the Polar Environment

3.1 Monitoring of Ice Sheet and Ice Shelf Mass Balance

Polar ice sheets and ice shelves are core cryospheric mass and energy storage carriers, with their mass balance and stability exerting decisive regulatory effects on global sea level and climate system evolution (**Chen et al., 2013; Manabe & Stouffer, 1995**). As key links between ice sheets and the ocean, ice shelves block inland ice flow while their basal melting and calving directly regulate ice sheet mass output (**Alley et al., 2021**). Major ice shelves globally are retreating and thinning—accelerated calving of Antarctica's Thwaites and Pine Island Ice Shelves drives Antarctic ice loss (**Li et al., 2022**), while Greenland's accelerated mass loss since the 1990s has released freshwater into the North Atlantic, suppressing thermohaline circulation (v**an den Broeke et al., 2017; Shen et al., 2020**).

Coupling of ice sheet basal dynamics and ice shelf erosion further impacts system stability. Antarctic subglacial lake drainage, a core subglacial hydrological process, transports meltwater to ice sheet downstream and grounding lines, altering basal lubrication, intensifying ice shelf melting, and triggering surface uplift or collapse with potential global climate and sea level impacts (**Smith et al., 2009**).

With centimeter-level elevation accuracy and high-density observation capabilities, ICESat-2 has established a multi-dimensional monitoring system covering ice sheet and ice shelf mass balance, stability, and hydrological processes. It advances research from single-parameter extraction to integrated multi-process, multi-scale, and multi-mechanism analysis, providing key support for understanding systematic change laws (**Khan et al., 2022**).

3.1.1 Ice Sheet Elevation Change and Mass Balance

Ice sheet and ice shelf changes fall into two categories defined by their driving mechanisms, with distinct spatial patterns: surface mass balance-driven changes show attenuated gradients and uniform thinning, whereas dynamic imbalance-driven changes feature strong spatial heterogeneity and stress-transmitted instabilities (**Fredensborg Hansen, 2021**).

To quantitatively analyze the above two types of ice sheet and ice shelf change processes, researchers have established a multi-level methodological framework centered on ice sheet elevation change detection, based on ICESat-2 combined with multi-source altimetry data such as CryoSat-2 (**Paolo et al., 2015; Zhang et al., 2017**). For changes driven by surface mass balance, the framework accurately extracts the elevation change rate of ice sheet areas by gridding and time-series fitting of photon data, while suppressing systematic errors through crossover analysis, thereby supporting the analysis of their dominant mechanisms. For changes driven by dynamic imbalance, it tracks local evolutionary characteristics via repeat orbit analysis and sliding window methods, and improves data signal-to-noise ratio through multi-level filtering, enabling refined characterization of such processes with strong heterogeneity and stress-transmitted instabilities (**Wang et al., 2024**).

Based on long-term time-series observations from ICESat-2 the overall accelerating loss trend and spatial heterogeneity characteristics of the Antarctic and Greenland Ice Sheets have been accurately characterized. Observation data show that the Antarctic Ice Sheet had an overall elevation decrease rate of –10.65±3.20 cm/yr between 2003 and 2020. The extreme melting event in 2019 further intensified ice mass loss (**Yang et al., 2022**). The

https://doi.org/10.5194/egusphere-2026-288
Preprint. Discussion started: 10 February 2026

Greenland Ice Sheet had a mass loss rate of –45.02±34.21 Gt/yr between 2019 and 2022 equivalent to a global sea level rise of approximately 0.12 mm/yr. Rising temperatures are the main driving factor (**Wang et al., 2024**). Notably the mass loss rate of peripheral glaciers in Greenland especially in the northern region has increased fourfold over the past two decades accounting for 11±2% of the total loss of the Greenland Ice Sheet. This highlights the characteristic of continuously increasing spatial heterogeneity of mass loss in the ice sheet system (**Khan et al., 2022**).

In terms of multi-source data collaboration and product validation ICESat-2 data show good consistency with radar altimetry data such as CryoSat-2. At a 5 km grid resolution and 30–60 day time window the elevation change trends of the Greenland Ice Sheet reflected by the two are highly consistent. The interannual difference is only 3.3±6.0 cm/yr which significantly improves the credibility of monitoring results (**Ravinder et al., 2024**). At the same time cross-validation with independent data such as ground-based GNSS measurements and airborne lidar has confirmed that the horizontal accuracy of ATL03 photon-level data from ICESat-2 is better than 5 cm. The accuracy of ATL06 elevation products reaches sub-decimeter level providing a solid foundation for the production and dynamic update of high-precision ice sheet DEMs (**Shen et al., 2022**). The currently achieved 500 m resolution DEM of the Antarctic Ice Sheet has a root mean square error controlled at –0.19 m and has annual update capability. It significantly improves the spatial details and timeliness of ice sheet topographic change monitoring.

3.1.2 Ice Shelf Stability Analysis

For the identification and morphological analysis of sub-ice shelf channels multi-beam laser profile terrain analysis technology uses the advantage of ICESat-2's six-beam dense spatial sampling to extract linear depression features on the ice shelf surface. It inverts the development process and thermal erosion effect of sub-ice channels combined with ice flow velocity data (**Siegfried and Fricker, 2018**).

Observations reveal that basal erosion processes play a core role in ice shelf dynamic adjustment. For example subglacial melt channels extend toward the grounding line at a rate of approximately 1 km/yr along the ice flow direction. The lateral migration rate reaches 70–80 m/yr and the basement erosion rate can reach 22 m/yr. This clearly reflects the dominant regulatory role of complex hydrodynamic processes at the base of ice shelves on ice shelf movement and structural stability (**Chartrand et al., 2020**). In addition for the inversion of ice thickness changes in ice shelf areas methods based on hydrostatic equilibrium principles are widely used. Ice thickness changes can be directly estimated through surface elevation combined with density differences between ice and seawater (**Chuter and Bamber, 2015; Griggs and Bamber, 2011**) providing key parameters for ice shelf mass balance and stability assessment.

In terms of key boundary monitoring ICESat-2 has significantly improved the spatial density and geometric accuracy of grounding line identification through repeat orbit observations. Collaborative analysis with differential interferometric synthetic aperture radar data can control the identification error of grounding line position within 0.39 km (**Li et al., 2020**) providing high-precision geometric constraints for characterizing grounding zone migration and dynamic development of subglacial melt channels. In the monitoring of ice shelf cracks and fracture processes the high-resolution elevation data from ICESat-2 provides important support for the extraction of three-dimensional crack morphology and tracking of propagation processes. Studies have shown that crack generation and propagation are jointly driven by basement fractures extreme meteorological events and changes in the thermal-dynamic state of ice

https://doi.org/10.5194/egusphere-2026-288
Preprint. Discussion started: 10 February 2026

shelves (Wang et al., 2021; Walker et al., 2021). By performing high-resolution elevation gradient and curvature analysis on ICESat-2 along-track elevation data and calculating the spatial variation of surface slope and curvature potential crack development areas can be accurately identified and their propagation paths can be tracked (Zhang et al., 2020).

In terms of numerical simulation and mechanism explanation the three-dimensional full Stokes ice flow model based on Elmer/Ice integrates BedMachine Antarctica terrain data and ICESat-2 ice flow velocity observations to achieve accurate simulation and verification of ice shelf dynamic processes (Guo et al., 2019). Typical case studies show that after the TWIT calving the Thwaites Eastern Ice Shelf (TEIS) formed a relatively independent dynamic system. The basal melting rate near the grounding line increased significantly confirming that changes in the physical state of the grounding line are key factors controlling the precursors of ice shelf calving (Alley et al., 2021).

3.1.3 Ice Sheet Hydrological Process Monitoring

In terms of subglacial lake monitoring, researchers first proposed a method for identifying subglacial lakes based on elevation change rate thresholds using first-generation ICESat data (Wingham et al., 2006), whose core idea is to calculate ice sheet surface elevation change rates, set reasonable thresholds, and combine visual interpretation to identify dynamic subglacial lakes and determine their boundaries. Subsequent studies further optimized the method by improving threshold adjustment and signal separation technologies (Stearns et al., 2008), and ICESat-2 has achieved accurate identification and refined boundary extraction of such lakes relying on its higher-precision photon-counting altimetry data under this framework.

For fine monitoring of subglacial lake water level changes, the repeat orbit elevation anomaly analysis method based on ICESat-2 captures filling and drainage events and their dynamic characteristics by analyzing time-series elevation data along preset orbits (Siegfried et al., 2021). Sliding time window and multi-source data fusion methods enhance hydrological event detection continuity by integrating adjacent observation period data, while the method of elevation anomaly difference inside and outside the lake extracts net elevation signals caused by subglacial lake activities by subtracting background area changes from target area anomalies (Scambos et al., 2011). For rapid hydrological activities, the maximum elevation change rate algorithm improves the detection capability of drainage and water storage events by extracting instantaneous change extremes between consecutive grid observations. In data quality control, multi-level filtering and residual elimination algorithms enhance the signal-to-noise ratio of elevation change signals through step-by-step screening based on quality indicators and iterative gridded surface fitting (Fair et al., 2020).

For supraglacial lake monitoring, ICESat-2 has realized high-precision identification and water depth inversion of supraglacial lakes in Antarctica and Greenland through the automatic processing algorithm of ATL03 photon data. With a maximum detection depth of 8.25 meters and bathymetric accuracy better than 0.32 meters (Xiao et al., 2023), this achievement significantly expands the application dimension of laser altimetry in ice sheet hydrological process monitoring.

https://doi.org/10.5194/egusphere-2026-288
Preprint. Discussion started: 10 February 2026

3.2 Multi-dimensional Sea Ice Parameter Retrieval

Accurately acquiring multi-dimensional core parameters including sea ice lead distribution, freeboard, thickness, melt pond morphology and snow depth is a prerequisite for analyzing sea ice evolution laws and quantifying its climate effects (**Perovich & Polashenski, 2012; Koo et al., 2023**). ICESat-2 has driven sea ice observation to advance from extensive extraction of single parameters to synergistic and accurate inversion of multi-parameters.

3.2.1 Lead Detection and Sea Ice Freeboard Retrieval

In terms of lead identification research methods have developed from early interpretation based on a single elevation threshold to a collaborative classification system of machine learning and deep learning integrating multi-dimensional features of photon point clouds and multi-source remote sensing information. By systematically extracting elevation distribution statistics photon rate echo waveform features and background noise levels from ICESat-2 photon data combined with spectral indices of high-resolution optical images and backscattering characteristics of SAR images a multi-modal feature space with strong separability has been constructed (**Pang et al., 2022; Liu et al., 2024**) (**Figure 5**).

Traditional supervised learning methods (such as random forests and support vector machines) have achieved robust classification of leads and sea ice based on this feature space. Deep learning methods based on convolutional neural networks and Transformer architectures have further improved the accuracy and generalization ability of lead boundary identification under complex ice-water mixing conditions through end-to-end feature learning and spatial context modeling (**Liang et al., 2022; Ricker et al., 2023**).

Sea ice freeboard retrieval hinges on accurate classification of sea ice and sea surface height segments, with ATL07/10-based photon classification algorithms distinguishing ice and water signals via signal intensity, photon distribution, elevation statistics and waveform feature analysis. However, current inversion faces multiple challenges: summer melt ponds are often misclassified as mixtures in ATL07, introducing type determination inconsistencies (**Tilling et al., 2020**); local non-crack segments used as sea surface references may cause estimation biases; ATL07/10's local height filter risks losing effective crack data and reducing spatial coverage; cloud attenuation can misclassify low-reflectivity regions as dark cracks (**Petty et al., 2021**). Notably, subsequent ATL07 versions excluded dark cracks from sea surface height calculations, lowering freeboard product spatial coverage by ~10–20% (**Kwok et al., 2021**).

In terms of detection and verification the method system has evolved from single optical verification to multi-source collaboration and intelligent identification. Early studies based on Sentinel-2 optical images proposed a crack ratio estimation method under strict spatiotemporal matching conditions. It was confirmed that ICESat-2 is reliable in identifying specular cracks but there is still great uncertainty in dark cracks and thin ice cracks (**Petty et al., 2021**). Subsequently SAR data was introduced to improve the accuracy of sea ice thickness inversion by improving the local sea surface height calculation algorithm (**Pang et al., 2022**).

In recent years, the integration of machine learning methods has significantly improved detection performance. A study constructing an unsupervised and supervised learning framework achieved a breakthrough in lead detection accuracy of 98.6% and recall rate of 91.8% (**Liu et al., 2025**). At the same time near-synchronous observations from

https://doi.org/10.5194/egusphere-2026-288
Preprint. Discussion started: 10 February 2026

SWOT and ICESat-2 have verified their high consistency in freeboard estimation (Kacimi et al., 2025) marking a new stage of multi-platform collaborative observation for sea ice parameter verification.

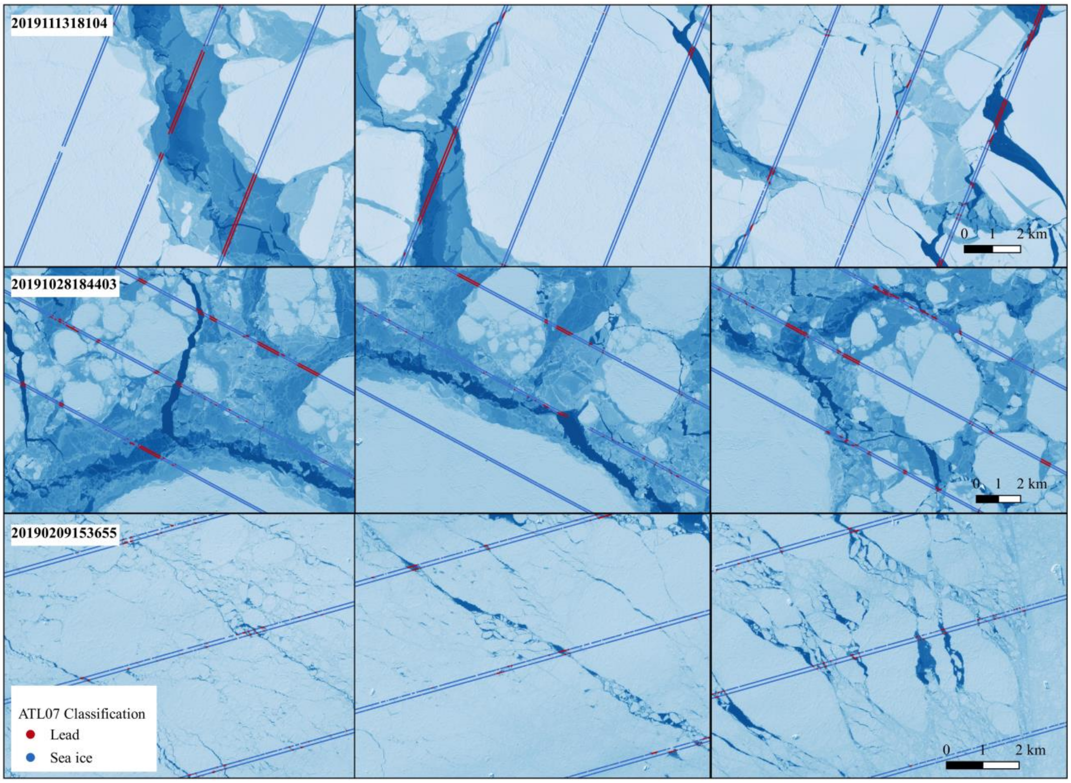

Figure 5. A Comparison of Sea Ice/Sea Surface Classification Between the ATL07 Decision Tree and a Machine Learning Approach Integrating Imagery.

3.2.2 Sea Ice Thickness Retrieval

A freeboard-thickness conversion theoretical framework based on hydrostatic equilibrium principles has been established. With ICESat-2 observed sea ice freeboard as the core input parameter, sea ice thickness is indirectly estimated by introducing snow depth correction terms and ice, snow, seawater density parameters (Studinger et al., 2024; Bocquet et al., 2023; Dong et al., 2023; Chen et al., 2023) (**Figure 6**).

In terms of data preprocessing and multi-source collaboration the accuracy and robustness of freeboard estimation have been improved by improving sea ice/seawater classification algorithms and local sea surface height determination methods. The extensive integration of multi-source data such as CryoSat-2 radar altimetry and passive microwave brightness temperature has significantly reduced the uncertainty of thickness inversion (Koo et al., 2021; Kacimi et al., 2020). Multi-platform verification results show that the thickness inverted by ICESat-2 has good consistency with IceBridge airborne observations SIMBA buoys and satellite products such as CryoSat-2 and HY-2B. Its systematic bias is mainly caused by the differential penetration effect of lasers in thin ice areas. This phenomenon has been quantitatively explained through pulse waveform analysis and radiative transfer models.

https://doi.org/10.5194/egusphere-2026-288
Preprint. Discussion started: 10 February 2026

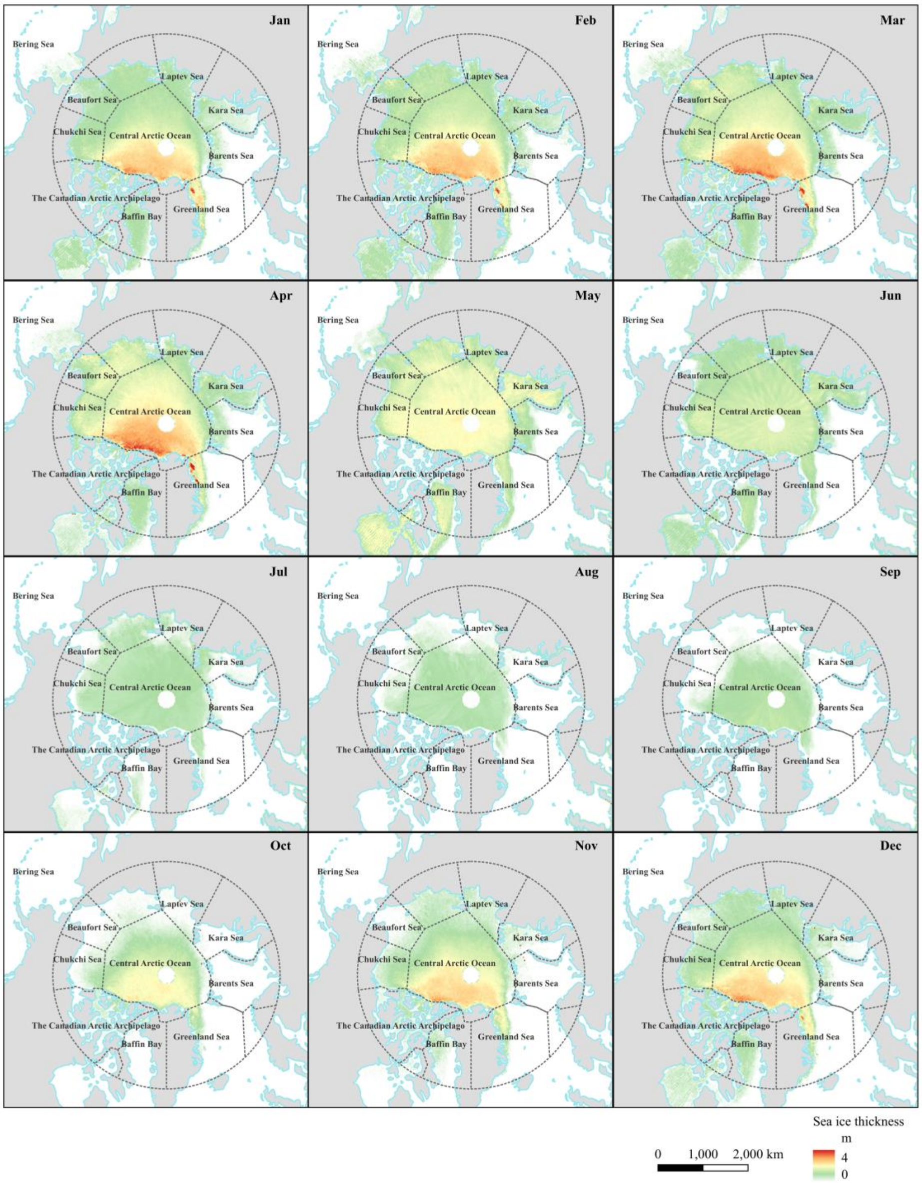

Figure 6. Arctic Monthly Sea Ice Thickness from 2013 to 2023 Derived from CryoSat-2, ICESat-2, and an Improved Snow Model

In terms of inversion method innovation the improved One-Layer Model (OLMi) has reduced the inversion uncertainty of Antarctic sea ice thickness to approximately 0.3 meters by optimizing freeboard calculation and reference sea surface determination (Xu et al., 2021). At the same time machine learning methods have been gradually applied to feature recognition and parameter optimization related to thickness. For example random forest models can realize automatic detection of detached fast ice with an identification accuracy of 99% (Koo et al., 2025). Current

https://doi.org/10.5194/egusphere-2026-288
Preprint. Discussion started: 10 February 2026

research further explores the application of deep learning in thickness inversion. By integrating multi-source remote sensing features and physical constraints the thickness estimation accuracy under complex ice conditions is improved.

In terms of scientific application and mechanism cognition the thickness products inverted by ICESat-2 have supported the drawing of spatial distribution maps of sea ice thickness in the Arctic and Antarctic (3–4 m in the Arctic and 2–3 m in the Antarctic) revealing their seasonal and interannual change characteristics (Shen et al., 2021; Petty et al., 2020). Research has further quantified the relative contributions of thermodynamic growth and dynamic thickening of sea ice. It has been found that the scope of the Antarctic marginal ice zone is significantly underestimated by approximately 7 times in traditional sea ice concentration algorithms highlighting the unique value of laser altimetry in finely depicting sea ice-ocean interactions (Brouwer et al., 2022). These observations not only deepen the understanding of sea ice change processes and climate effects but also provide a centimeter-level accuracy elevation benchmark for global cryosphere remote sensing monitoring playing an irreplaceable role in Earth system change research (Magruder et al., 2024).

3.2.3 Melt Pond Detection

The spatial distribution, depth, and geometric morphology of melt ponds are jointly regulated by ice type, surface roughness, and melting stage (Dawson et al., 2022). In recent years, research using high-precision laser altimetry data such as ICESat-2 has advanced notably in multi-source data collaboration, algorithm innovation, and parameter inversion (Webster et al., 2022). Melt pond detection integrates ICESat-2's photon penetration capability and multi-spectral images' spectral response characteristics, forming a complete observation chain from micro-scale water depth inversion and macro-scale spatial mapping to climate effect analysis.

In terms of detection and inversion methods, the UMD-RDA algorithm based on ICESat-2 photon point clouds has achieved centimeter-level resolution detection of sea ice microtopography, revealing structural differences between multi-year and first-year ice. At the point scale, laser photons penetrate clear water, enabling water depth inversion (accuracy ~0.1 m) via analyzing echo time differences between water surfaces and pond bottoms, with accuracy affected by water turbidity, ice internal structure, and pond bottom morphology (Farrell et al., 2020). For coverage and morphology monitoring, the improved normalized difference water index classification combined with dual-surface elevation tracking algorithm realizes synergistic inversion of melt pond coverage (seasonal peak: 16%±6%) and depth (seasonal peak: 0.97 m±0.51 m). Additionally, the density-dimension dual-segmentation algorithm achieves automatic 0.7 m-resolution detection and feature extraction of melt ponds, showing good operational potential (Buckley et al., 2023; Tilling et al., 2018).

At the regional scale, multi-spectral images identify melt pond ranges via normalized difference water index and spectral features; collaboration with ICESat-2 data enables acquisition of their three-dimensional morphology and spatial distribution, as well as quantification of their impacts on ice surface albedo and ice-albedo feedback intensity (Buckley et al., 2023). Due to their optical and thermodynamic properties falling between high-albedo ice and low-albedo open water, melt ponds are often misclassified as leads or thin ice in traditional methods, affecting the reliability of sea ice concentration, freeboard, and mass balance estimation (Dawson et al., 2022). To address this, current research constructs multi-modal deep learning models integrating laser elevation, multi-spectral, and thermal infrared data, classifying melt ponds as an independent land cover type.

For multi-source data fusion and verification, combining spectral characteristics of high-resolution optical images improves melt pond boundary identification accuracy, and medium-resolution optical data is found to systematically underestimate melt pond coverage (**Tilling et al., 2020**). Meanwhile, cross-validation between CryoSat-2 and ICESat-2 reveals radar signals' elevation underestimation on melt pond surfaces due to complex scattering, highlighting the complementary value of laser and radar observations (**Dawson & Landy, 2023; Kwok et al., 2020c**).

3.2.4 Snow Depth

Currently snow depth estimation has formed an inversion system integrating multi-sensor collaboration physical mechanisms and data-driven methods. Three mainstream method systems have been developed with ICESat-2 as the core (**Yan et al., 2024; Glissenaar et al., 2021**).

The first is the radar-laser collaborative inversion method. Based on synchronous observations from CryoSat-2 and ICESat-2 it utilizes the characteristic that radar signals can penetrate dry snow layers while laser signals are mainly reflected from the snow layer surface. By accurately registering the observed elevations of the two the radar penetration depth is directly estimated and then the snow depth is calculated (**Kwok et al., 2018; Saha et al., 2025**). This method has been systematically verified in the Arctic sea ice area revealing the seasonal change of snow depth from approximately 9 cm in October to 19 cm in April. The snow depth in multi-year ice areas is significantly higher than that in first-year ice (**Kwok et al., 2020a**). However there is an underestimation of 2–4 cm in areas without open leads. The inversion accuracy is jointly affected by ice surface roughness snow salinity and tide correction errors (**Fredensborg Hansen et al., 2024**). Further integrating L-band passive microwave radiation can realize the joint optimization inversion of sea ice thickness and snow depth effectively reducing the uncertainty caused by parameter coupling (**Zhou et al., 2018**).

The second is the laser altimetry differential method. Based on photon elevation data such as ICESat-2 ATL06/ATL08 the seasonal snow depth is directly extracted by differencing with high-precision snow-free DEM. This method performs well in low-slope non-vegetated areas. The basin-scale snow depth inversion accuracy can reach 0.18–0.33 m (RMSE) and it has a high correlation with measured snow depth in flat bare areas (R^2 up to 0.88) (**Besso et al., 2024; Deschamps-Berger et al., 2023; Feng et al., 2025**). However in complex terrain forested areas and glacier surfaces the inversion accuracy decreases significantly affected by terrain occlusion vegetation penetration and seasonal evolution of ice surfaces (**Enderlin et al., 2022**).

The third is the multi-source data fusion and machine learning method. Snow depth estimation is performed by integrating passive microwave optical remote sensing and reanalysis data combined with radiative transfer models or machine learning algorithms. Passive microwave radiation information is incorporated into the modeling framework. Its brightness temperature is sensitive to snow layer microphysical properties and can establish a correlation with snow depth through radiative transfer models or machine learning methods (**Saha et al., 2025**). Optical remote sensing combined with radiative transfer models can achieve high-precision snow depth inversion under suitable conditions. The average difference between the simplified scheme and buoy-measured snow depth is only 4.1 cm (**Wang et al., 2023**). Machine learning methods can effectively integrate passive microwave brightness temperature laser altimetry features and other auxiliary data to realize daily snow depth estimation in the Arctic with an RMSE of about 9–10 cm showing strong spatiotemporal modeling and generalization capabilities (**Sun-Mack et al., 2025**).

https://doi.org/10.5194/egusphere-2026-288
Preprint. Discussion started: 10 February 2026

Furthermore multi-source data fusion strategies adopt dynamic assimilation and feature fusion methods such as observation updates based on time-series filtering and cross-modal feature extraction and mapping using neural networks. They integrate complementary information from radar altimetry laser altimetry passive microwave and reanalysis data effectively suppressing systematic biases caused by sensor limitations seasonal changes and spatial heterogeneity (Zeng et al., 2018; Hu et al., 2022; Kacimi et al., 2022).

3.3 Holistic Changes of the Polar Environment and Multi-element Collaborative Applications

Constructing a holistic understanding of polar cryosphere systematic changes is key to clarifying intra-sphere and cross-sphere coupling mechanisms and linking local-regional-global cognition. As an initial forcing factor, climate warming reshapes atmospheric circulation and ocean thermal structure, acting on cryosphere core components to trigger chain responses that feed back to sphere interactions, forming feedback loops that amplify or regulate climate signals (Zeng et al., 2018; Saha et al., 2025; Hu et al., 2022) (**Figure 7**). Examples include ice sheet meltwater altering ocean stratification to regulate sea ice dynamics, and sea ice reduction with melt pond development lowering albedo to drive atmospheric-sea ice-energy positive feedback. The cryosphere is also deeply intertwined with ecological and atmospheric spheres (Quartly et al., 2019; Zhang et al., 2023). ICESat-2 provides key data for analyzing multi-sphere and multi-element collaborative coupling mechanisms (Ham et al., 2019). It captures subtle changes in ice sheets, sea ice, vegetation and other elements, supporting quantification of interaction intensity, revelation of evolution laws and construction of holistic cognition.

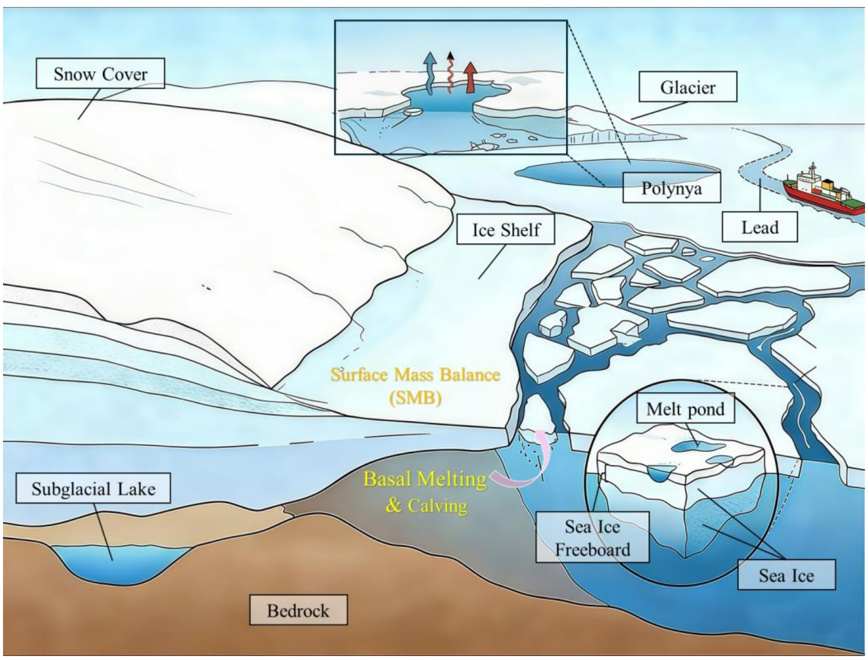

Figure 7. Schematic diagram of polar environmental elements. It illustrates the typical ice-ocean system environmental elements in polar regions covering ice units such as ice sheets ice shelves glaciers and sea ice.

https://doi.org/10.5194/egusphere-2026-288
Preprint. Discussion started: 10 February 2026

3.3.1 Analysis of Ice Sheet/Ice Shelf-Ocean-Atmosphere Coupling Mechanisms

Under climate warming, rising polar temperatures intensify ice sheet surface melting, altering ice surface runoff paths and reshaping the ice sheet's internal hydrological cycle (Scambos et al., 2011; Smith et al., 2009). Increased frequency and intensity of subglacial lake filling and drainage change lubrication conditions between the ice sheet base and bedrock, reducing ice flow resistance and accelerating ice flow, forming a multi-element collaborative response chain of temperature rise, enhanced hydrological activity, and dynamic strengthening (Alley et al., 2021).

Accelerated ice flow triggers further multi-element chain reactions. It increases ice shelf mass output to the ocean, intensifying interactions between the ice shelf front and warm circumpolar currents and raising ice shelf basal erosion rates. Meanwhile, continuous ice shelf thinning and structural damage cause inland grounding line migration, weakening overall ice sheet stability (Siegfried and Fricker, 2018). This multi-element chain collaborative response profoundly affects polar mass balance and global sea level change trends.

ICESat-2's high-precision time-series data enables accurate quantification of multi-element collaborative effect intensity and key correlation parameters. For instance, its ice flow velocity and subglacial lake water level data capture temporal synchronization and spatial correspondence between Antarctic subglacial lake drainage events and sudden ice flow acceleration, clarifying subglacial hydrological processes' regulatory effect on ice sheet dynamics (Herzfeld et al., 2023).

Tracking Greenland Ice Sheet melt pond coverage, surface albedo, and melting rate changes reveals that a 10% increase in melt pond coverage reduces surface albedo by 8%-12%, boosting surface melting rate by 15%-20% (Niehaus et al., 2025; Painter et al., 2016). Additionally, ICESat-2 ice sheet elevation data separates contributions of dynamic thinning and surface accumulation/ablation processes, enabling accurate attribution of ice sheet change mechanisms and clarifying their contribution to global sea level rise (Khan et al., 2022; Brunt et al., 2019).

3.3.2 Analysis of Sea Ice-Ocean-Atmosphere Coupling Mechanisms

As a key interface for polar cryosphere-ocean-atmosphere interactions, sea ice drives multi-element collaborative evolution via energy exchange regulation and material cycle coupling. In terms of energy exchange, polar warming-induced rapid snow melting and extensive ice surface melt ponds lower ice surface albedo. This enhances polar solar radiation absorption efficiency, strengthens sensible heat, latent heat and radiative energy exchange between sea and atmosphere, and accelerates sea ice thermodynamic ablation (Perovich & Polashenski, 2012). Meanwhile, increased sea ice fragmentation and large-scale lead development expand direct ocean-atmosphere contact area, amplifying energy exchange intensity. This forms a positive feedback cycle of warming, sea ice ablation and enhanced energy exchange, promoting atmospheric-sea ice-energy collaborative intensification and polar warming (Curry et al., 1995; Marcq et al., 2012).

In material cycle, high-salinity brine released during sea ice growth strengthens ocean vertical mixing, boosting deep warm water upward transport that feeds back to sea ice basal erosion. Abundant freshwater from sea ice ablation alters upper ocean stratification stability, inhibiting deep warm water upward transport and forming negative feedback on sea ice melting—together maintaining the dynamic balance of the polar ocean-sea ice system (Deems et al., 2013; Painter et al., 2016). Additionally, sea ice has close cross-component connections with ice sheets and ice shelves, highlighting polar environment holism. Ocean surface temperature and salinity changes from sea ice ablation affect

https://doi.org/10.5194/egusphere-2026-288
Preprint. Discussion started: 10 February 2026

ice shelf front current distribution and regulate ice shelf basal erosion rate. Freshwater from ice sheet and ice shelf melting alters sea ice growth conditions, inhibiting its formation and development, forming an ice sheet-ice shelf-sea ice-ocean multi-element cross-component collaborative evolution pattern (Frei et al., 2012).

ICESat-2 data supports systematic analysis of seasonal and interannual dynamic characteristics of sea ice growth and ablation, as well as their collaborative correlations with atmospheric temperature, ocean currents and other elements (Tilling et al., 2020; Buckley et al., 2023). Combined with surface albedo, snow depth and other auxiliary parameters, it enables ice surface energy balance closure calculation and improves polar energy-sea ice-atmosphere multi-element cycle models. Freshwater release flux estimated from high-resolution sea ice thickness data accurately characterizes the impact of ice melting on ocean surface salinity, clarifying polar freshwater-ocean-thermohaline circulation collaborative mechanisms.

ICESat-2 along-track thickness information allows accurate evaluation of seasonal and interannual sea ice mass balance changes at regional and basin scales. Combined with sea ice movement trajectory data, it accounts for ice mass budget in specific sea areas (Herzfeld et al., 2023). Research results on energy and material fluxes based on its high-precision data provide key parameterization scheme verification for ocean-ice-atmosphere coupling models, improving model reliability in simulating polar multi-element collaborative evolution (Dawson et al., 2018).

3.3.3 Analysis of Polar Cryosphere-Ecology-Atmosphere Coupling Mechanisms

Holistic polar environment changes manifest not only in cryosphere-ocean-atmosphere core interactions but also in cryosphere-ecology-atmosphere multi-element collaborative evolution. In tundra ecosystem research, ICESat-2 vegetation canopy height data is a key structural parameter linked to tundra carbon-nitrogen cycle efficiency, permafrost thermal stability and habitat quality, providing critical initial data and verification basis for building cryosphere-ecology-permafrost multi-element coupling models (Zhang et al., 2025).

Meanwhile, ICESat-2 snow depth and canopy height data facilitate accurate analysis of their interaction mechanisms. For instance, tall shrubs capture and retain snow, altering winter soil thermal insulation, which in turn affects permafrost thermal state and melting depth. This provides a new perspective for understanding vegetation-snow-soil-permafrost cascading collaborative effects and revealing polar ecology-cryosphere evolution laws (Bisson et al., 2021).

In polar atmospheric process research, ICESat-2 derived atmospheric parameter data fills gaps in traditional passive remote sensing for refined polar boundary layer vertical structure observation. Analyzing photon vertical distribution in atmospheric scattering layers enables accurate inversion of aerosol extinction coefficient profiles and cloud vertical structure parameters, clarifying vertical transport paths and distribution laws of aerosols, water vapor and clouds in the polar boundary layer (Urban et al., 2008; Zhang et al., 2023). This quantifies their contribution to cloud condensation nuclei formation and regulation of surface net radiation. Measured data-based vertical process constraints make up for climate model deficiencies in simulating polar cloud-radiation-aerosol collaborative forcing, improving model accuracy in simulating polar cryosphere-atmosphere coupling.

https://doi.org/10.5194/egusphere-2026-288
Preprint. Discussion started: 10 February 2026

4. Key Uncertainties and Technical Breakthrough Paths in ICESat-2 Cryosphere Observations

Early algorithms have improved accuracy by addressing photon signal processing refraction correction and multi-source data fusion. However breakthroughs in addressing snow depth spatiotemporal heterogeneity complex terrain interference and observation system limitations remain insufficient. This chapter systematically sorts out the initial resolution of dominant uncertainties through ICESat-2 algorithm evolution. It deeply traces the core uncertainty sources in snow depth estimation complex terrain observation and observation system limitations. It clarifies future technical development directions providing theoretical and technical support for analyzing the mechanisms of polar system change.

4.1 ICESat-2 Algorithm Evolution Initial Resolution of Uncertainties and Practical Achievements

4.1.1 Core Algorithm Improvements in the Academic Community

Table 2 Core Algorithm Innovations in the Academic Community

Associated Products	Uncertainty Issues	Improved Algorithms	Optimization Effects and Conclusions	References
ATL07	Cloud attenuation reduces photon rate leading to misclassification of dark leads. This causes the reference value of sea surface height to be too high and freeboard estimation to be too low.	Construct an automatic sea surface type classification algorithm based on multi-parameters such as photon rate distribution width and background noise.	Version R003 only uses specular lead data. The coverage rate decreases by 10–20% but the average freeboard increases by 0–4 cm.	Kwok et al, 2021
ATL10 NESOSIM v1.1	Snow spatiotemporal heterogeneity and simplified model assumptions lead to insufficient sea ice thickness inversion accuracy.	NESOSIM v1.1 introduces atmospheric blowing snow loss terms ERA5 snowfall forcing calibrated by CloudSat and recalibrates with OIB snow depth data.	The upgrade of ATL10 rel003~005 freeboard improves thickness inversion accuracy. It enhances consistency with CryoSat-2 results.	Petty et al., 2023
ATL03 ATL07	Significant noise photon interference. It is difficult to accurately extract sea ice signal photons affecting the accuracy of sea ice change monitoring.	Propose an Adaptive Clustering and Kernel Density Estimation method to accurately separate noise and sea ice signal photons from photon cloud data.	It outperforms traditional algorithms under different signal-to-noise ratio conditions. The accuracy and F-score reach 0.97. The inverted height has a correlation R ＞ 0.97 with ATM airborne data.	Liu et al., 2023
ATLAS Underwater terrain-related products	Deviations between model assumptions and actual scenarios lead to systematic displacement errors	A refraction correction method based on ray tracing and JONSWAP wave spectrum. Reconstruct the wave profile to calculate the air/sea surface intersection of seabed photons.	Realize photon-level 3D coordinate compensation. Overcome the limitation of vertical correction. Improve bathymetric accuracy in shallow water areas and under fluctuating sea surface conditions	Zhang et al., 2022

https://doi.org/10.5194/egusphere-2026-288
Preprint. Discussion started: 10 February 2026

Aiming at observational bottlenecks such as sea ice freeboard estimation bias and insufficient bathymetric accuracy in early ICESat-2 data products caused by cloud interference noise photons and model simplification the academic community has carried out algorithm innovations focusing on core links such as signal processing and model adaptation (Chen et al., 2022). Through the implementation and application transformation of technical schemes it has helped continuously improve the accuracy of polar environmental observation data providing key support for subsequent product iterations (**Table 2**).

4.1.2 Multi-version Iteration of Official Algorithms

Official version iteration integrates academic algorithm innovations into global optimized products, translating technical breakthroughs into large-scale applications.

In the elevation product iteration from V03 to V07, the official launched multi-dimensional collaborative upgrades focusing on enhancing data absolute accuracy and reliability (Kwok et al., 2022). On one hand, it integrated high-precision tidal parameters, modern reference frameworks and high-resolution DEM, while updating atmospheric and oceanic correction models to systematically address comprehensive uncertainties from terrain and atmospheric interference, absorbing academic technical insights on complex scene correction. On the other hand, it upgraded the quality control system, expanding control dimensions from basic engineering markers to photon-level parameters, adding a dynamic uncertainty assessment module to strengthen signal extraction in high signal-to-noise ratio environments. Supplementary core indicators such as geometric parameters and photon weights improved product data dimensions and application flexibility, providing standardized data support for subsequent uncertainty tracing and in-depth analysis (Bagnardi et al., 2021).

In the sea ice product iteration from V04 to V06, the official took reference benchmark unification as the core, linking algorithm correction, quality control upgrades and function expansion to achieve global performance optimization (Kwok et al., 2021b). To address freeboard inversion bias caused by inconsistent early tidal benchmarks, it built a unified and reliable geometric foundation through full-link tidal benchmark unification and parameter transmission, laying a standardized premise for centimeter-level freeboard inversion. Absorbing academic automated processing experience, it upgraded quality control from traditional manual inspection to an automated multi-level filtering system, which accurately identifies and removes invalid and abnormal data by combining multi-dimensional quality markers and auxiliary data to ensure product purity. It also corrected sea ice segment length calculation methods, calibrated first photon bias, applied dynamic atmospheric correction models to improve inversion accuracy, expanded product parameter dimensions, deepened integration with external remote sensing data, and enhanced product adaptability in climatology and air-sea interaction research (Neumann et al., 2022), forming a standardized and highly compatible observation product system.

4.2 Tracing Core Uncertainties in ICESat-2 Cryosphere Observations

Although early algorithm iterations have resolved some dominant uncertainties residual errors and potential interference still exist in snow depth estimation complex terrain observation and observation system limitations.

https://doi.org/10.5194/egusphere-2026-288
Preprint. Discussion started: 10 February 2026

4.2.1 Uncertainty Sources in Snow Depth Estimation

Snow depth is a core parameter for sea ice thickness inversion and ice sheet mass balance assessment, with its uncertainties directly affecting downstream results. These uncertainties manifest in three dimensions.

First, interference from snow's spatiotemporal heterogeneity (Petty et al., 2023). Polar snow forms complex layered structures and dynamic density distributions under blowing snow, wind-driven accumulation and snowmelt refreezing. Its physical characteristics vary by region and season, limiting the universality of single models. Early models incorporated blowing snow loss terms but failed to fully characterize spatiotemporal heterogeneity, with local snow depth fluctuations and compaction-induced photon interaction changes during snowmelt causing estimation biases.

Second, observation system signal recognition errors (Liu et al., 2023). Photon signals are prone to cloud, aerosol scattering and background noise interference, with unresolved confusion in snow-ice and snow-atmosphere interface classification. Cloud attenuation may misclassify snow surface photons as ice surface ones, underestimating snow depth, while high-reflectivity snow amplifies noise and impairs effective photon extraction—driving continuous optimization of denoising algorithms.

Third, deviations between model assumptions and actual scenarios (Zhang et al., 2022). Traditional snow depth inversion relies on hydrostatic equilibrium or empirical models, ignoring processes like spatiotemporal snowfall differences. Most parameters depend on regional calibration data, lacking global applicability. Even with optimized density parameters, fixed assumptions conflict with actual snow density, and low snowfall data spatial resolution leads to inaccurate accumulation estimation and systematic biases.

4.2.2 Uncertainty Sources in Complex Terrain Observations

Complex terrains such as ice sheet margins, ice shelf regions with dense crevasses, and mountain glaciers have become high-uncertainty areas due to their special geometric characteristics and poor compatibility with observation systems. Their impacts run through the entire processes of signal reception and data processing:

On the one hand, topographic geometric characteristics induce multiple interferences (Li et al., 2024). Steep terrain causes laser spot occlusion, forming observational blind spots. Complex structures trigger multi-path reflection of photons, generating spurious signals that interfere with the extraction of true elevation—this is also the core background for the optimization of the AV-OPTICS model for near-seabed terrain. Meanwhile, the slope effect alters the spot projection area; when the slope is large, signals disperse, reducing observation resolution and accuracy. The narrow structures and steep sidewalls in areas with dense crevasses further exacerbate this problem.

On the other hand, there is a mismatch between observation systems and terrain resolution (Kwok et al., 2023). Inherent limitations in the along-track sampling interval and spot size of ICESat-2 prevent accurate coverage of small-scale, highly heterogeneous terrains, leading to the loss of topographic details. Moreover, atmospheric correction models for complex terrains are mostly based on flat surface assumptions, ignoring the impact of topographic relief on atmospheric scattering and refraction. Insufficient correction further amplifies uncertainties, which is also an important reason for the continuous optimization of the atmospheric correction model in the ATL03 version.

4.2.3 Uncertainty Sources in Observation System Limitations

Observation system inherent limitations and on-orbit interference are core uncertainty sources in cryosphere observations, manifesting mainly in three dimensions: payload performance, on-orbit operation, and observation coverage.

First, inherent limitations of payload performance. The photon-counting lidar payload has technical shortcomings, with weak ability to capture faint signals. On low-albedo ice-snow surfaces, thin snow cover or shadowed areas, signals are easily attenuated, making effective extraction difficult and causing inversion errors (Neumann et al., 2019). Fixed laser spot size and emission frequency limit spatial sampling density, failing to adapt to small-scale terrain and fine snow structure observation needs, restricting accuracy improvement. Additionally, payload measurement noise and systematic bias slightly affect photon positioning and elevation inversion, becoming inherent uncertainty factors.

Second, impacts of on-orbit operation interference. Satellite attitude jitter, orbit deviation and other dynamic interferences are unavoidable, shifting laser irradiation positions from preset paths and indirectly reducing photon positioning accuracy (Magruder et al., 2021). Such deviations accumulate in complex terrain and large-scale continuous observations, amplifying overall errors. Meanwhile, ionospheric and atmospheric disturbances alter laser signal propagation paths, interfering with signal reception and analysis and increasing data processing uncertainty.

Third, limitations of observation coverage and timeliness. Constrained by observation perspective, scanning range and orbit design, large-scale cryosphere observations have time intervals, making high-frequency dynamic monitoring difficult. Short-time scale processes like snow ablation, sea ice deformation and glacier movement are easily missed, leading to incomplete capture of cryosphere changes (Markus et al., 2017). Moreover, single-payload observation mode poorly adapts to complex weather; heavy clouds, snowfall and other conditions degrade data quality or even cause interruptions, forming blind spots and exacerbating uncertainties.

4.3 Technical Paths and Future Directions for ICESat-2 Cryosphere Observations

4.3.1 In-depth Breakthrough Paths for Uncertainties in Snow Depth Estimation

Build on early snow depth models and signal processing algorithms, advancing collaboration across signal recognition, model mechanism and data fusion to address snow heterogeneity, signal interference and model deviation.

At the signal processing level, upgrade adaptive photon classification and denoising technologies (Liu et al., 2023). Integrate deep learning semantic segmentation, random forests and other technologies into existing algorithms to construct a multi-feature classification model based on photon intensity, spatial distribution and temporal changes, distinguishing snow surface, ice surface photons and noise accurately. Develop dynamic threshold algorithms that adjust parameters by regional signal-to-noise ratio to reduce misfiltering of effective snow photons, and use convolutional neural networks to extract spatial texture features for complex snow scenarios.

At the model optimization level, construct a multi-process dynamic snow model (Petty et al., 2023b). Enhance parameterized characterization of atmospheric blowing snow and snowmelt refreezing processes based on existing models. Integrate satellite snow vertical structure data to optimize spatiotemporal dynamic schemes for snow density,

https://doi.org/10.5194/egusphere-2026-288
Preprint. Discussion started: 10 February 2026

replacing fixed density assumptions. Establish regional and seasonal calibration systems by fusing high-resolution snowfall data and airborne measurements to improve global applicability and mitigate biases from snow heterogeneity.

At the multi-source fusion level, build a collaborative observation system (Zhang et al., 2022b). Combine high-precision laser altimetry data, wide-coverage microwave remote sensing data and ground observation data. Adopt data assimilation technology to achieve high-precision, wide-coverage snow depth inversion, leveraging multi-source data complementarity to reduce single-observation uncertainty and overcome limitations of early single data sources.

4.3.2 In-depth Breakthrough Paths for Uncertainties in Complex Terrain Observation

Address terrain occlusion, multi-path reflection and resolution mismatch in small or complex terrain observation through observation strategies, signal processing and platform collaboration.

At the observation strategy level, adaptively optimize satellite observation parameters (Kwok et al., 2023). Adopt encrypted orbits in key regions to reduce along-track sampling intervals, optimize laser spot size and emission frequency to improve small-scale terrain resolution. Develop dynamic observation modes that adjust emission parameters based on terrain slope, roughness and other prior information to mitigate occlusion and multi-path reflection impacts at the source.

At the signal processing level, develop terrain-adaptive correction algorithms (Li et al., 2024). Integrate high-resolution DEM prior information into existing models to identify occluded areas and multi-path reflection risk zones, performing targeted photon signal correction. Introduce slope correction models to adjust photon elevation calculation methods and eliminate slope-induced systematic biases. Use ray tracing to simulate photon propagation paths, correct false signals in steep terrain, and develop morphological clustering algorithms to extract crack wall true elevation accurately.

At the platform collaboration level, construct a three-dimensional observation network (Bagnardi et al., 2021). Integrate laser altimetry data with high-resolution optical and SAR satellite macro-structural information to identify blind spots and interference sources. Utilize UAVs and airborne lidar for close-range high-precision observations, providing correction samples for laser data and forming an air-space-ground collaborative system to resolve uncertainties.

4.3.3 Targeted Breakthrough Paths for Observation System Limitations

Address payload inherent limitations, on-orbit interference and resolution mismatch through payload technology upgrades, on-orbit control optimization and observation mode adjustment, systematically improving data accuracy.

Upgrade payload technology to break hardware bottlenecks (Kwok et al., 2022). Enhance weak signal detection sensitivity for low-albedo and thin snow scenarios, reduce signal attenuation errors. Upgrade laser emission and reception modules to shrink spot size and increase frequency while maintaining observation range, improving spatial sampling density for small-scale terrain. Integrate high-precision attitude measurement and correction modules to monitor and correct on-orbit attitude jitter and orbit deviation in real time, enhancing data reliability.

Optimize on-orbit control and preprocessing. Build a collaborative processing system via intelligent control and edge computing, adopting intelligent on-orbit control algorithms to adjust observation angles and paths based on snow type and terrain complexity. Conduct high-frequency repeated observations in key regions to compensate for large-scale observation time intervals and reduce omission of short-scale cryosphere changes (Magruder et al., 2024).

https://doi.org/10.5194/egusphere-2026-288
Preprint. Discussion started: 10 February 2026

Strengthen on-orbit preprocessing capabilities to complete weak signal enhancement, outlier removal and uncertainty prediction in advance, prioritizing high-value data transmission to reduce ground processing pressure.

Adjust observation modes through main-auxiliary payload linkage. Combine optimized lidar with microwave radiometers and hyperspectral imagers to leverage multi-payload complementarity (Magruder et al., 2021). Use microwave radiometers' all-weather advantages for cloud-covered scenario calibration, and hyperspectral imagers' spectral recognition capabilities to improve photon classification accuracy in weak signal scenarios, alleviating system limitations systematically.

4.3.4 Future Direction Multi-dimensional Technology Fusion Empowers Accurate Cryosphere Observations

Advance cryosphere observation capabilities through deep coupling of intelligent data processing, multi-source remote sensing fusion, single-satellite multi-payload integration and on-satellite-off-satellite collaborative processing, building a high-precision, full-dimension, all-weather and intelligent observation system.

Develop intelligent data processing based on deep learning and reinforcement learning, building end-to-end photon signal processing models adaptable to snow cover, complex terrain and fluctuating sea surfaces (Yang et al., 2025). Complete signal classification, noise removal and outlier elimination without preset parameters, adopting scenario-specific strategies—using background rate parameters for non-polar night scenarios and solar radiation-independent photon characteristics for polar nights. Integrate physical mechanisms and data-driven hybrid modeling, embedding snow evolution and terrain undulation processes into the framework to upgrade from phenomenon fitting to mechanism explanation.

Promote multi-source remote sensing fusion by integrating optimized laser data with SAR, optical and gravity satellite observations (Liu et al., 2025). Use data assimilation for collaborative inversion of elevation, humidity, density and mass balance. Leverage optical satellites' macro texture recognition and SAR satellites' all-weather advantages to locate blind spots and correct multi-path reflection false signals, taking high-precision elevation data as the core reference to generate high-resolution application products for practical scenarios, forming an algorithm optimization-data complementarity-application implementation closed loop.

Realize single-satellite multi-payload integration in upgraded satellite models, integrating lidar, hyperspectral imagers and microwave radiometers for simultaneous acquisition of elevation, spectral characteristics, thermal radiation intensity and humidity (Pang et al., 2023). Reduce spatiotemporal registration errors in multi-platform fusion, and reserve expansion interfaces for flexible addition of interferometric measurement and thermal infrared detection payloads to adapt to environmental changes and application demands.

Advance on-satellite-off-satellite collaboration: optimize on-satellite preprocessing to extract core parameters such as sea ice thickness and concentration, reducing invalid data transmission; integrate off-satellite SAR ice type identification, optical melt pond distribution and meteorological data to generate 100-meter high-resolution navigation risk assessment maps (Zhao et al., 2024). Construct intelligent route planning systems based on multi-dimensional data and ship parameters, and assimilate sea ice dynamic models with ocean current and atmospheric circulation predictions for short-term sea ice change early warning (Ricker et al., 2023). Use long-term time-series data for

https://doi.org/10.5194/egusphere-2026-288
Preprint. Discussion started: 10 February 2026

seasonal waterway prediction and fleet deployment, and dynamically monitor port-surrounding sea ice to assess infrastructure damage risks (Petty et al., 2021).

5. Summary and Outlook

This review takes laser altimetry satellite technology as the core anchor, systematically collates its technical characteristics and polar environmental application progress, and constructs a problem-driven analytical framework around three core scientific questions. It combs through technical evolution context, polar environmental parameter retrieval, observational uncertainties and corresponding technical breakthrough paths in a holistic manner, integrating scattered research findings in the field, refining core operational laws, and addressing the fragmented adaptation dilemma between existing technologies and polar application scenarios.

Regarding the mechanistic connection between technical innovations and inversion bottlenecks, this review clarifies the adaptive logic between advanced laser altimetry technologies and cryospheric parameter retrieval demands, elaborates on how multi-beam configurations compensate for spatial coverage deficiencies of single-beam systems and the inherent advantages of photon-counting technology in polar weak-signal environments. It constructs a complete technical chain spanning observation technology, data products and cryospheric adaptation, integrating remote sensing technology with cryospheric scientific questions via a clear paradigm.

Centering on the integration of observational results and systematic cognition construction, this review clarifies the core logic of building holistic cryospheric cognition via satellite data. It systematically integrates insights into polar ice sheet and ice shelf stability, as well as multi-dimensional sea ice parameter retrieval, to construct a holistic scientific understanding of the systematic change laws of the polar environment.

For key uncertainty sources and resolution paths, this review accurately traces core error sources in snow depth estimation, complex terrain observation and system limitations, and establishes a three-dimensional breakthrough system integrating signal processing optimization, model refinement and multi-source collaboration, while proposing actionable uncertainty control schemes. These findings provide practical support for improving satellite data reliability and managing observational uncertainties.

Looking ahead, based on the sorted research context and technical bottlenecks, the next generation of laser altimetry satellites should rely on the synergy of four core technologies: intelligent data processing, multi-source remote sensing fusion, single-satellite multi-payload integration, and on-satellite-off-satellite collaborative processing. This synergy will break through current limitations in snow and subglacial terrain detection, realize polar multi-parameter simultaneous observation, hourly revisit and global coverage, and support global climate change response and Arctic navigation safety, advancing cryospheric observation towards higher precision, full dimensionality and deeper mechanistic understanding.

Acknowledgments

The research was supported by the Fundamental Research Funds for the Central Universities, China, grant number 2042022dx0001 and the Natural Science Foundation of Wuhan, grant number 2024040701010030.

https://doi.org/10.5194/egusphere-2026-288
Preprint. Discussion started: 10 February 2026

References

1. Abdalati, W., Zwally, H.J., Bindschadler, R., Csatho, B., Farrell, S.L., Fricker, H.A., 2010. The ICESat-2 Laser Altimetry Mission. Proceedings of the IEEE 98(5), 735-751. https://doi.org/10.1109/JPROC.2009.2034765.
2. Alley, K.E., Wild, C.T., Luckman, A., Scambos, T.A., Truffer, M., Pettit, E.C., 2021. Two decades of dynamic change and progressive destabilization on the Thwaites Eastern Ice Shelf. The Cryosphere 15, 5187–5203, https://doi.org/10.5194/tc-15-5187-2021.
3. Andersen, O. B., Knudsen, P., and Stenseng, L., 2015. The DTU13 MSS (Mean Sea Surface) and MDT (Mean Dynamic Topography) from 20 Years of Satellite Altimetry. In: Jin, S., Barzaghi, R. (eds) IGFS 2014. International Association of Geodesy Symposia, 144. Springer, Cham. https://doi.org/10.1007/1345_2015_182.
4. Bagnardi, M., Kurtz, N. T., Petty, A. A., Kwok, R., 2021. Sea surface height anomalies of the Arctic Ocean from ICESat-2: A first examination and comparisons with CryoSat-2. Geophysical Research Letters 48, e2021GL093155. https://doi.org/10.1029/2021GL093155.
5. Besso, H., Shean, D., Lundquist, J.D., 2024. Mountain snow depth retrievals from customized processing of ICESat-2 satellite laser altimetry. Remote Sensing of Environment 300, 113843. https://doi.org/10.1016/j.rse.2023.113843.
6. Bisson, K.M., Cael, B.B., 2021. How are under ice phytoplankton related to sea ice in the Southern Ocean? Geophysical Research Letters 48, e2021GL095051.https://doi.org/10.1029/2021GL095051.
7. Bocquet, M., Fleury, S., Piras, F., Rinne, E., Sallila, H., Garnier, F., Rémy, F., 2023. Arctic sea ice radar freeboard retrieval from the European Remote-Sensing Satellite (ERS-2) using altimetry: toward sea ice thickness observation from 1995 to 2021. The Cryosphere 17, 3013–3039. https://doi.org/10.5194/tc-17-3013-2023.
8. Bolch, T., Sandberg Sørensen, L., Simonsen, S.B., Mölg, N., Machguth, H., Rastner, P., Paul, F., 2013. Mass loss of Greenland's glaciers and ice caps 2003–2008 revealed from ICESat data.Geophysical. Research Letters 40, 875–881, https://10.1002/grl.50270.
9. Brouwer, J., Fraser, A.D., Murphy, D.J., Wongpan, P., Alberello, A., Kohout, A., 2022. Altimetric observation of wave attenuation through the Antarctic marginal ice zone using ICESat-2. The Cryosphere 16, 2325–2353. https://doi.org/10.5194/tc-16-2325-2022.
10. Brunt, K. M., Smith, B. E., Sutterley, T. C., Kurtz, N. T., Neumann, T. A., 2021. Comparisons of satellite and airborne altimetry with ground-based data from the interior of the Antarctic ice sheet. Geophysical Research Letters 48, e2020GL090572. https://doi.org/10.1029/2020GL090572.
11. Brunt, K.M., Neumann, T.A., Smith, B.E., 2019. Assessment of ICESat-2 ice sheet surface heights, based on comparisons over the interior of the Antarctic ice sheet. Geophysical Research Letters 46, 13072–13078. https://doi.org/10.1029/2019GL084886.
12. Buckley, E.M., Farrell, S.L., Herzfeld, U.C., Webster, M.A., Trantow, T., Baney, O.N., et al., 2023. Observing the evolution of summer melt on multiyear sea ice with ICESat-2 and Sentinel-2. The Cryosphere 17, 3695–3719, https://doi.org/10.5194/tc-17-3695-2023.
13. Chartrand, A.M., Howat, I.M., 2020. Basal channel evolution on the Getz Ice Shelf, West Antarctica. Journal of Geophysical Research: Earth Surface 125, e2019JF005293. https://doi.org/10.1029/2019JF005293.
14. Chen, G., Zhang, Z., Rose, S. K., Andersen, O. B., Zhang, S., Jin, T., 2022. A new Arctic MSS model derived from combined Cryosat-2 and ICESat observations. International Journal of Digital Earth 15(1), 2202–2222. https://doi.org/10.1080/17538947.2022.2153181.
15. Chen, J., Wilson, C., Tapley, B., 2013. Contribution of ice sheet and mountain glacier melt to recent sea level rise. Nature Geoscience 6, 549–552. https://doi.org/10.1038/ngeo1829.
16. Chen, Y., Lei, R., Zhao, X., Wu, S., Liu, Y., Fan, P., Ji, Q., Zhang, P., Pang, X., 2023. A new sea ice concentration product in the polar regions derived from the FengYun-3 MWRI sensors. Earth System Science Data 15, 3223–3242. https://doi.org/10.5194/essd-15-3223-2023.

https://doi.org/10.5194/egusphere-2026-288
Preprint. Discussion started: 10 February 2026

17. Chuter, S.J., Bamber, J.L., 2015. Antarctic ice shelf thickness from CryoSat-2 radar altimetry. Geophysical Research Letters 42(10), 721–10,729. https://doi.org/10.1002/2015GL066515.

18. Connor, L.N., Farrell, S.L., McAdoo, D.C., Krabill, W.B., Manizade, S., 2013. Validating ICESat Over Thick Sea Ice in the Northern Canada Basin. IEEE Transactions on Geoscience and Remote Sensing 51(4), 2188-2200. https://doi: 10.1109/TGRS.2012.2211603.

19. Curry, J.A., Schramm, J.L., Ebert, E.E., 1995. Sea Ice-Albedo Climate Feedback Mechanism. Climate, 8, 240–247. https://doi.org/10.1175/1520-0442(1995)008<0240:SIACFM>2.0.CO;2.

20. Dawson, G., Landy, J., Tsamados, M., Komarov, A. S., Howell, S., Heorton, H., Krumpen, T., 2022. A 10 year record of Arctic summer sea ice freeboard from CryoSat-2, Remote Sensing of Environment 268, 112744. https://doi.org/10.1016/j.rse.2021.112744.

21. Dawson, G.J., Landy, J.C., 2023. Comparing elevation and backscatter retrievals from CryoSat-2 and ICESat-2 over Arctic summer sea ice. The Cryosphere 17, 4165–4178, https://doi.org/10.5194/tc-17-4165-2023.

22. Dawson, N., Broxton, P., and Zeng, X., 2018. Evaluation of Remotely Sensed Snow Water Equivalent and Snow Cover Extent over the Contiguous United States. Journal of Hydrometeor 19, 1777–1791. https://doi.org/10.1175/jhm-d-18-0007.1.

23. Deems, J.S., Painter, T.H., Finnegan, D.C., 2013. Lidar Measurement of Snow Depth: A Review. Journal of Glaciology 59(215), 467–479. https://doi.org/10.3189/2013JoG12J154.

24. Deschamps-Berger, C., Gascoin, S., Shean, D., Besso, H., Guiot, A., López-Moreno, J. I., 2023. Evaluation of snow depth retrievals from ICESat-2 using airborne laser-scanning data. The Cryosphere 17, 2779–2792. https://doi.org/10.5194/tc-17-2779-2023.

25. Ding, Y.J., Mu, C.C., Wu, T.H., Hu, G.J,, Zou, D.F., Wang, D., et al., 2021. Increasing cryospheric hazards in a warming climate. Earth-Science Reviews 213, 103500. https://doi.org/10.1016/j.earscirev.2020.103500.

26. Dong, Z., Shi, L., Lin, M., Jia, Y., Zeng, T., Wu, S., 2023. Feasibility of retrieving Arctic sea ice thickness from the Chinese HY-2B Ku-band radar altimeter. The Cryosphere 17, 1389–1410. https://doi.org/10.5194/tc-17-1389-2023.

27. Enderlin, E.M., Elkin, C.M., Gendreau, M., Marshall, H.P., O'Neel, S., McNeil, C., 2022. Uncertainty of ICESat-2 ATL06-and ATL08-derived snow depths for glacierized and vegetated mountain regions. Remote Sensing of Environment 283, 113307. https://doi.org/10.1016/j.rse.2022.113307.

28. Fair, Z., Flanner, M., Brunt, K. M., Fricker, H. A., Gardner, A., 2020. Using ICESat-2 and Operation IceBridge altimetry for supraglacial lake depth retrievals. The Cryosphere 14, 4253–4263. https://doi.org/10.5194/tc-14-4253-202.

29. Farrell, S.L., Duncan, K., Buckley, E.M., Richter-Menge, J., and Li, R., 2020. Mapping Sea Ice Surface Topography in High Fidelity With ICESat-2. Geophys. Res. Lett 47, e2020GL090708. https://doi.org/10.1029/2020GL090708.

30. Farrell, S.L., Laxon, S.W., McAdoo, D.C., Yi, D., Zwally, H. J., 2009. Five years of Arctic sea ice freeboard measurements from the Ice, Cloud and land Elevation Satellite. Geophysical Research Letters 114, C04008, https://10.1029/2008JC005074.

31. Feng, D., Che, T., Wang, G., Dai, L., Gao, L., Jiang, Y., et al., 2025. Seasonal snow depth dataset over flat terrains in the Northern Hemisphere based on ICESat-2 data from 2018 to 2020. International Journal of Digital Earth 18(1), 2528632. https://doi.org/10.1080/17538947.2025.2528632.

32. Fredensborg Hansen, R.M., Rinne, E., Farrell, S.L., Skourup, H., 2021. Estimation of degree of sea ice ridging in the Bay of Bothnia based on geolocated photon heights from ICESat-2. The Cryosphere 15, 2511–2529. https://doi.org/10.5194/tc-15-2511-2021.

33. Fredensborg Hansen, R.M., Skourup, H., Rinne, E., Høyland, K.V., Landy, J.C., Merkouriadi, I., et al., 2024. Arctic freeboard and snow depth from near-coincident CryoSat-2 and ICESat-2 (CRYO2ICE) observations: A first examination of winter sea ice during 2020–2022. Earth and Space Science 11, e2023EA003313. https://doi.org/10.1029/2023EA003313.

34. Frei, A., Tedesco, M., Lee, S., Foster, J., Hall, D. K., Kelly, R., et al., 2012. A Review of Global Satellite-Derived Snow Products. Advances in Space Research 50(8), 1007–1029. https://doi.org/10.1016/j.asr.2011.12.021.

35. Gardner,A.S., Moholdt, G.,Wouters, B., Wolken, G.J., Burgess, D.O., Sharp, M.J., et al., 2011. LabineSharply increased mass loss from glaciers and ice caps in the Canadian Arctic ArchipelagoNature 473(7347), 357-360. https://doi.org/10.1038/nature10089.

36. Glissenaar, I.A., Landy, J.C., Petty, A.A., Kurtz, N.T., Stroeve, J.C., 2021. Impacts of snow data and processing methods on the interpretation of long-term changes in Baffin Bay early spring sea ice thickness. The Cryosphere 15, 4909–4927. https://doi.org/10.5194/tc-15-4909-2021.

37. Goosse, H., Kay, J.E., Armour, K.C., Bodas-Salcedo, A., Chepfer, H., Docquier, D., et al., 2018. Quantifying climate feedbacks in polar regions. Nature Communications 9, 1919. https://doi.org/10.1038/s41467-018-04173-0.

38. Griggs, J.A., Bambe,r J.L., 2011. Antarctic ice-shelf thickness from satellite radar altimetry. Journal of Glaciology 57(203):485-498. https://doi.org/10.3189/002214311796905659.

39. Guo, X., Zhao, L., Gladstone, R. M., Sun, S., Moore, J. C., 2019. Simulated retreat of Jakobshavn Isbræ during the 21st century. The Cryosphere 13, 3139–3153. https://doi.org/10.5194/tc-13-3139-2019.

40. Ham, Y.G., Kim, J.H. & Luo, J.J., 2019. Deep learning for multi-year ENSO forecasts. Nature 573, 568–572. https://doi.org/10.1038/s41586-019-1559-7.

41. Herzfeld, U.C., Trantow, T. Han, M., Buckley, H.E., Farrell, S.L., Lawson, M., 2023. Automated Detection and Depth Determination of Melt Ponds on Sea Ice in ICESat-2 ATLAS Data—The Density-Dimension Algorithm for Bifurcating Sea-Ice Reflectors (DDA-Bifurcate-Seaice). IEEE Transactions on Geoscience and Remote Sensing 61, 4300922. https://10.1109/TGRS.2023.3268073.

42. Howat, I.M., Smith, B.E., Joughin I., Scambos, T.A., 2008. Rates of southeast Greenland ice volume loss from combined ICESat and ASTER observations. Geophysical Research Letters 35, L17505, https://10.1029/2008GL034496.

43. Hu, X., Hao, X., Wang, J., Huang, G., H. Yang, L.Q., 2021. Can the Depth of Seasonal Snow be Estimated From ICESat-2 Products: A Case Investigation in Altay, Northwest China. IEEE Geoscience and Remote Sensing Letters 19(1-5), 2000405. https://doi.org/10.1109/LGRS.2021.3078805.

44. Hu, Y., Lu, X., Zeng, X., Stamnes, S.A., Neuman, T.A., Kurtz, N.T., 2022. Deriving Snow Depth From ICESat-2 Lidar Multiple Scattering Measurements. Frontiers in Remote Sensing 3, 2022. https://doi.org/10.3389/frsen.2022.855159.

45. Jahn, A., Holland, M.M., Kay, J.E., 2024. Projections of an ice-free Arctic Ocean. Nature Reviews Earth &Environment 5, 164–176. https://doi.org/10.1038/s43017-023-00515-9.

46. Kääb, A., Berthier, E., Nuth, C. Gardelle, J., Arnaud, Y., 2012.Contrasting patterns of early twenty-first-century glacier mass change in the Himalayas. Nature 488, 495–498. https://doi.org/10.1038/nature11324.

47. Kacimi, S., Jaruwatanadilok, S., Kwok, R., 2025.SWOT observations over sea ice: A first look.Geophysical Research Letters 52, e2025GL116079.https://doi.org/10.1029/2025GL116079.

48. Kacimi, S., Kwok, R., 2020. The Antarctic sea ice cover from ICESat-2 and CryoSat-2: freeboard, snow depth, and ice thickness. The Cryosphere 14, 4453–4474, https://doi.org/10.5194/tc-14-4453-2020.

49. Kacimi, S., Kwok, R., 2022. Arctic snow depth, ice thickness, and volume from ICESat-2 and CryoSat-2: 2018–2021. Geophysical Research Letters, 49, e2021GL097448. https://doi.org/10.1029/2021GL097448.

50. Khan, S.A., Colgan, W., Neumann, T.A., van den Broeke, M.R., Brunt, K.M., Noël, B., et al., 2022. Accelerating ice loss from peripheral glaciers in North Greenland. Geophysical Research Letters 49, e2022GL098915. https://doi.org/10.1029/2022GL098915.

51. Koo, Y., Xie, H., Kurtz, N.T., Ackley, S.F., Wang, W., 2023. Sea ice surface type classification of ICESat-2 ATL07 data by using data-driven machine learning model: Ross Sea, Antarctic as an example. Remote Sensing Environment 296, 113726. https://doi.org/10.1016/j.rse.2023.113726.

https://doi.org/10.5194/egusphere-2026-288
Preprint. Discussion started: 10 February 2026

52. Koo, Y., Xie, H., Meier, W.N., Stephen F.A., Nathan, T.K., 2025. Detection of multi-year ex-fast ice in the Weddell Sea, Antarctica, using ICESat-2 satellite altimeter data. Remote Sensing of Environment 325, 114750. https://doi.org/10.1016/j.rse.2025.114750.

53. Koo, Y.H., Lei, R., Cheng, Y., Cheng, B., Xie, H., Hoppmann, M., 2021. Estimation of thermodynamic and dynamic contributions to sea ice growth in the Central Arctic using ICESat-2 and MOSAiC SIMBA buoy data. Remote Sensing of Environment 267, 112730. https://doi.org/10.1016/j.rse.2021.112730.

54. Kwok, R., A. Petty, M. Bagnardi, N. T. Kurtz, G. F. Cunningham, A. Ivanoff., 2021. Refining the sea surface identification approach for determining freeboard in the ICESat-2 sea ice products, The Cryosphere, 15, 821–833, https://doi.org/10.5194/tc-15-821-2021.

55. Kwok, R., Cunningham, G. F., Wensnahan, M., Rigor, I., Zwally, H. J., Yi, D., 2009. Thinning and volume loss of the Arctic Ocean sea ice cover: 2003–2008. Geophysical Research Letters 114, C07005, https://10.1029/2009JC005312.

56. Kwok, R., Cunningham, G.F., Kacimi, S., Webster, M.A., Kurtz, N.T., Petty, A.A. 2020c. Decay of the snow cover over Arctic sea ice from ICESat-2 acquisitions during summer melt in 2019. Geophysical Research Letters 47, e2020GL088209. https://doi.org/10.1029/2020GL088209.

57. Kwok, R., Kacimi, S., Webster, M.A., Kurtz, N. T., Petty, A.A., 2020a. Arctic snow depth and sea ice thickness from ICESat-2 and CryoSat-2 freeboards: A first examination. Journal of Geophysical Research: Oceans 125, e2019JC016008. https://doi.org/10.1029/2019JC016008.

58. Kwok, R., Markus, T., 2018. Potential basin-scale estimates of Arctic snow depth with sea ice freeboards from CryoSat-2 and ICESat-2: An exploratory analysis. Advances in Space Research 62(6), 1243-1250. https://doi.org/10.1016/j.asr.2017.09.007.

59. Kwok, R., Markus, T., Kurtz, N.T., Petty, A. A., Neumann, T.A., Farrell, S.L., et al., 2019. Surface height and sea ice freeboard of the Arctic Ocean from ICESat-2: Characteristics and early results. Journal of Geophysical Research: Oceans 124, 6942–6959. https://doi.org/10.1029/2019JC015486.

60. Kwok, R., Petty, A., Cunningham, G., Markus, T., Hancock III, D.W., Ivanoff, A., et al., 2023. ATLAS/ICESat-2 L3A Sea Ice Height, Version 6. [Indicate subset used]. Boulder, Colorado USA. NASA National Snow and Ice Data Center Distributed Active Archive Center. https://doi.org/10.5067/ATLAS/ATL07.006.

61. Kwok, R., Petty, A.A., Bagnardi, M., Kurtz, N.T., Cunningham, G F., Ivanoff, A., et al., 2021b. Refining the sea surface identification approach for determining freeboards in the ICESat-2 sea ice products. The Cryosphere 15, 821–833. https://doi.org/10.5194/tc-15-821-2021.

62. Kwok, R., Petty, A.A., Cunningham, G., Hancock, D., Ivanoff, A., Wimert, J., et al., 2020b. Ice, Cloud, and land Elevation Satellite-2 project: Algorithm Theoretical Basis Document (ATBD) for sea ice products (ATL07/ATL10), release 003.https://doi.org/10.5067/UAZPI91070H4.

63. Lefsky, M.A., Harding, D.J., Keller, M., Cohen, W.B., Carabajal, C.C., Del Bom Espirito-Santo, F., et al., 2005. Estimates of forest canopy height and aboveground biomass using ICESat. Geophysical Research Letters 32, L22S02, https://10.1029/2005GL023971.

64. Li, P., Xu, Y., Zhao, Y., Liang, K., Si, Y., 2024. Denoising of Photon-Counting LiDAR Bathymetry Based on Adaptive Variable OPTICS Model and Its Accuracy Assessment. Remote Sensing 16, 3438. https://doi.org/10.3390/rs16183438.

65. Li, T., Dawson, G. J., Chuter, S. J., Bamber, J. L., 2020. Mapping the grounding zone of Larsen C Ice Shelf, Antarctica, from ICESat-2 laser altimetry. The Cryosphere 14, 3629–3643, https://doi.org/10.5194/tc-14-3629-2020.

66. Li, T., Dawson, G.J., Chuter, S.J., Bamber, J.L., 2022. A high-resolution Antarctic grounding zone product from ICESat-2 laser altimetry, Earth System Science Data 14, 535–557, https://doi.org/10.5194/essd-14-535-2022.

67. Li, W., Hsu, C., Tedesco, M., 2024. Advancing Arctic Sea Ice Remote Sensing with AI and Deep Learning: Opportunities and Challenges. Remote Sensing 16, 3764. https://doi.org/10.3390/rs16203764.

68. Liang, Z.Y, Pang, X.P, Ji, Q.Q, X. Zhao, X., Li, G.Y., Chen, Y.Z., 2022. An Entropy-Weighted Network for Polar Sea Ice Open Lead Detection From Sentinel-1 SAR Images. IEEE Transactions on Geoscience and Remote Sensing 60, 4304714. https://doi.org/10.1109/TGRS.2022.3169892.

https://doi.org/10.5194/egusphere-2026-288
Preprint. Discussion started: 10 February 2026

69. Liu, J., Xie, H., Guo, Y., Tong, X., Li, P., 2022. A Sea Ice Concentration Estimation Methodology Utilizing ICESat-2 Photon-Counting Laser Altimeter in the Arctic. Remote Sensing 14, 1130. https://doi.org/10.3390/rs14051130.

70. Liu, J.P., Chen, Z.Q., Hu Y.Y., Zhang, Y.Y., Ding, Y.F., Cheng, X., et al., 2019. Towards reliable Arctic sea ice prediction using multivariate data assimilation. Science Bulletin 64(1), 63-72. https://doi.org/10.1016/j.scib.2018.11.018.

71. Liu, W., Liu, T., Jin, J, Li., W, Jiang., 2023. Adaptive Clustering-Based Method for ICESat-2 Sea Ice Retrieval. IEEE Transactions on Geoscience and Remote Sensing 61, 4301814. https://doi.org/10.1109/TGRS.2023.3287909.

72. Liu, W.X., Tsamados, M., Petty A., Jin, T.Y., Chen, W.B., Stroeve, J., 2025. Enhanced sea ice classification for ICESat-2 using combined unsupervised and supervised machine learning. Remote Sensing of Environment 318, 114607. https://doi.org/10.1016/j.rse.2025.114607.

73. Liu, Z., and Schweiger, A., 2024. ICESat-2 Shows Sea Ice Leads Have Little Overall Effects on the Arctic Cloudiness in Cold Months. Climate 37, 4045–4058. https://doi.org/10.1175/JCLI-D-23-0285.1.

74. Magruder, L.A., Brunt, K.M., & Alonzo, M., 2020. Early ICESat-2 on-orbit geolocation validation using ground-based corner cube retro-reflectors. Remote Sensing, 12, 3653. https://doi.org/10.3390/rs12213653.

75. Magruder, L.A., Farrell, S.L., Neuenschwander, A., Duncanson, L., Csatho, B., Kacimi, S., et al., 2024. Monitoring Earth's climate variables with satellite laser altimetry. Nature Reviews Earth Environment 5, 120–136. https://doi.org/10.1038/s43017-023-00508-8.

76. Manabe, S., Stouffer, R., 1995. Simulation of abrupt climate change induced by freshwater input to the North Atlantic Ocean. Nature 378, 165–167. https://doi.org/10.1038/378165a0.

77. Marcq, S., and Weiss, J., 2012. Influence of sea ice lead-width distribution on turbulent heat transfer between the ocean and the atmosphere. The Cryosphere 6, 143–156. https://doi.org/10.5194/tc-6-143-2012.

78. Markus, T., Neumann, T., Martino, A., Abdalati, W., Brunt, K., Csatho, B., et al., 2017. The Ice, Cloud, and land Elevation Satellite-2 (ICESat-2): Science requirements, concept, and implementation. Remote Sensing of Environment 190, 260–273. https://doi.org/10.1016/j.rse.2016.12.029.

79. Michael, P., Karen, L.S., and Lorenzo, M.P., 2021. Arctic amplification of climate change: a review of underlying mechanisms. Environmental Research Letters 16, 9. https://doi.org/10.1088/1748-9326/ac1c29.

80. Moholdt, G., Nuth,C, Hagen, J.O., Kohler, J., 2010. Recent elevation changes of Svalbard glaciers derived from ICESat laser altimetry. Remote Sensing of Environment 114(11), 2756-2767. https://doi.org/10.1016/j.rse.2010.06.008.

81. Neuenschwander, A.L., Pitts K.L., Jelley B.P., Robbins J., Klotz B., Popescu S.C., 2021. ATLAS/ICESat-2 L3A land and vegetation height, version 5. NASA National Snow and Ice Data Center Distributed Active Archive Center, Boulder, Colorado USA. https://doi.org/10.5067/ATLAS/ATL08.005.

82. Neuenschwander, A.L., Urban, T.J, Gutierrez, R., Schutz, B.E., 2008. Characterization of ICESat/GLAS waveforms over terrestrial ecosystems: Implications for vegetation mapping. Geophysical Research Letters 113, G02S03. https://10.1029/2007JG000557.

83. Neumann, T.A., Brenner, A., Hancock, D., Robbins, J., Gibbons, A., Lee, J., 2022. Ice, Cloud, and Land Elevation Satellite (ICESat-2) Project Algorithm Theoretical Basis Document (ATBD) for Global Geolocated Photons ATL03, Version 6. ICESat-2 Project. https://doi.org/10.5067/GA5KCLJT7LOT.

84. Neumann, T.A., Martino, A.J., Markus, T., Bae, S., Bock, M.R., Brenner, A.C., et al., 2019. The Ice, Cloud, and land Elevation Satellite—2 mission: A global geolocated photon product derived from the Advanced Topographic Laser Altimeter System. Remote Sensing of Environment 233, 111325. https://doi.org/10.1016/j.rse.2019.111325.

85. Painter, T.H., Berisford, D.F., Boardman, J.W., Bormann, K.J., Deems, J.S., Gehrke, F., et al. 2016. The Airborne Snow Observatory: Fusion of Scanning Lidar, Imaging Spectrometer, and Physically-Based Modeling for Mapping Snow Water Equivalent and Snow Albedo. Remote Sensing Environment 184, 139–152. https://doi.org/10.1016/j.rse.2016.06.018.

https://doi.org/10.5194/egusphere-2026-288
Preprint. Discussion started: 10 February 2026

86. Pang, X., Zhang, C., Ji, Q., Chen, Y., Zhen, Z., Zhu, Y., et al., 2023. Analysis of sea ice conditions and navigability in the Arctic Northeast Passage during the summer from 2002-2021. Geo-Spatial Information Science 26(3), 465–479. https://doi.org/10.1080/10095020.2022.2124128.

87. Pang, X.P., Chen, Y.Z., Ji, Q., Li, G.Y., Shi, L.J., Lan, M.S., et al., 2022. An Improved Algorithm for the Retrieval of the Antarctic Sea Ice Freeboard and Thickness from ICESat-2 Altimeter Data. Remote Sensing 14, 1069. https://doi.org/10.3390/rs14051069.

88. Paolo, F.S., Fricker, H.A., Padman, L., 2015. Volume loss from Antarctic ice shelves is accelerating.Science348,327-331. https://doi.org/10.1126/science.aa0940.

89. Perovich, D.K. and Polashenski, C., 2012. Albedo Evolution of Seasonal Arctic Sea Ice, Geophysical Research Letters 39, L08501. https://doi.org/10.1029/2012GL051432.

90. Petty, A.A., Bagnardi, M., Kurtz, N.T., Tilling, R., Fons, S., Armitage, T., et al., 2021. Assessment of ICESat-2 sea ice surface classification with Sentinel-2 imagery: Implications for freeboard and new estimates of lead and floe geometry. Earth and Space Science 8, e2020EA001491. https://doi.org/10.1029/2020EA001491.

91. Petty, A.A., Keeney, N., Cabaj, A., Kushner, P., and Bagnardi, M., 2023. Winter Arctic sea ice thickness from ICESat-2: upgrades to freeboard and snow loading estimates and an assessment of the first three winters of data collection. The Cryosphere 17, 127–156. https://doi.org/10.5194/tc-17-127-2023.

92. Petty, A.A., Keeney, N., Cabaj, A., Kushner, P., and Bagnardi, M., 2023b. Winter Arctic sea ice thickness from ICESat-2: upgrades to freeboard and snow loading estimates and an assessment of the first three winters of data collection. The Cryosphere 17, 127–156. https://doi.org/10.5194/tc-17-127-2023.

93. Petty, A.A., Kurtz, N.T., Kwok, R., Markus, T., Neumann, T.A, 2020. Winter Arctic sea ice thickness from ICESat-2 freeboards. Journal of Geophysical Research: Oceans 125, e2019JC015764. https://doi.org/10.1029/2019JC015764.

94. Pritchard, H.D, Ligtenberg, S.R.M, Fricker, H.A., Vaughan, D.G., van den Broeke, M.R., Padman, L., 2012. Antarctic ice-sheet loss driven by basal melting of ice shelves. Nature 484, 502–505. https://doi.org/10.1038/nature10968.

95. Qu, M., Zhao, X., Pang, X.P., Lei, R.B., 2022. Review of Arctic Sea Ice Leads:Physics and Remote Sensing. Advance in Earth Sciences 37(4), 382-391.(In Chinese with English abstract).

96. Quartly, G.D., Rinne, E., Passaro, M., Andersen, O.B., Dinardo, S., Fleury, S., et al., 2019. Retrieving Sea Level and Freeboard in the Arctic: A Review of Current Radar Altimetry Methodologies and Future Perspectives. Remote Sensing 11, 881. https://doi.org/10.3390/rs11070881.

97. Ravinder, N., Shepherd, A., Otosaka, I., Slater, T., Muir, A., Gilbert, L., 2024. Greenland Ice Sheet elevation change from CryoSat-2 and ICESat-2. Geophysical Research Letters 51, e2024GL110822. https://doi.org/10.1029/2024GL110822.

98. Ricker, R., Fons, S., Jutila, A., Hutter, N., Duncan, K., Farrell, S. L., et al., 2023. Linking scales of sea ice surface topography: evaluation of ICESat-2 measurements with coincident helicopter laser scanning during MOSAiC. The Cryosphere 17, 1411–1429. https://doi.org/10.5194/tc-17-1411-2023.

99. Saha, M., Stroeve, J., Isleifson, D., Yackel, J., Nandan, V., Landy, J. C., et al., 2025. Snow depth estimation on leadless landfast ice using Cryo2Ice satellite observations. The Cryosphere 19, 325–346. https://doi.org/10.5194/tc-19-325-2025.

100. Scambos, T.A., Berthier, E., Shuman, C.A., 2011. The triggering of subglacial lake drainage during rapid glacier drawdown: Crane Glacier, Antarctic Peninsula. Annals of Glaciology 52(59),74-82. https://doi.org/10.3189/172756411799096204.

101. Serreze, M.C., and Stroeve, J., 2015. Arctic sea ice trends, variability and implications for seasonal ice forecasting. Philosophical Transactions of the Royal Society A Mathematical Physical and Engineering Sciences, 37320140159. http://doi.org/10.1098/rsta.2014.0159.

102. Shen, X., Ke, C.Q., Fan, Y., Drolma, L., 2022. A new digital elevation model (DEM) dataset of the entire Antarctic continent derived from ICESat-2. Earth System Science Data 14, 3075–3089, https://doi.org/10.5194/essd-14-3075-2022.

103. Shen, X., Ke, C.Q., Wang, Q., Zhang, J., L. Zhang, S.X., 2021. Assessment of Arctic Sea Ice Thickness Estimates from ICESat-2 Using IceBird Airborne Measurements. In IEEE Transactions on Geoscience and Remote Sensing 59(5), 3764-3775. https://doi.org/10.1109/TGRS.2020.3022945.

104. Shen, X., Ke, C.Q., Yu, X., Cai, Y., Fan, Y., 2020. Evaluation of Ice, Cloud, And Land Elevation Satellite-2 (ICESat-2) land ice surface heights using Airborne Topographic Mapper (ATM) data in Antarctica. International Journal of Remote Sensing 42(7), 2556–2573. https://doi.org/10.1080/01431161.2020.1856962.

105. Siegfried, M.R., Fricker, H.A., 2021. Illuminating active subglacial lake processes with ICESat-2 laser altimetryGeophysical Research Letters 48, e2020GL091089. https://doi.org/10.1029/2020GL091089.

106. Siegfried. M.R., Fricker. H.A., 2018. Thirteen years of subglacial lake activity in Antarctica from multi-mission satellite altimetry. Annals of Glaciology 59(76), 42-55. https://doi.org/10.1017/aog.2017.36.

107. Smith, B., Fricker, H.A., Holschuh, N., Gardner, A.S., Adusumilli, S., Brunt, K.M., 2019. Land ice height-retrieval algorithm for NASA's ICESat-2 photon-counting laser altimeter. Remote Sensing Environment 233, 111352, https://doi.org/10.1016/j.rse.2019.111352 .

108. Smith, B.E., Fricker, H.A., Joughin, I.R., Tulaczyk, S., 2009. An inventory of active subglacial lakes in Antarctica detected by ICESat (2003–2008). Journal of Glaciology 55(192), 573-595. https://doi.org/10.3189/002214309789470879.

109. Song, L., Song, C., Song, S., Luo, T., Chen, K., Liu, Y., Zhang, L.K., 2023. Integrating ICESat-2 altimetry and machine learning to estimate the seasonal water level and storage variations of national-scale lakes in ChinaRemote Sensing Environment 294, 113657. https://doi.org/10.1016/j.rse.2023.113657.

110. Spinhirne, J.D., Palm, S.P., Hart, W.D., Hlavka, D.L., Welton, E.J., 2005. Cloud and aerosol measurements from GLAS: Overview and initial results. Geophysical Research Letters 32, L22S03. https://10.1029/2005GL023507.

111. Stearns, L., Smith, B. & Hamilton, G., 2008. Increased flow speed on a large East Antarctic outlet glacier caused by subglacial floods. Nature Geoscience 1, 827–831. https://doi.org/10.1038/ngeo356.

112. Studinger, M., Smith, B.E., Kurtz, N., Petty, A., Sutterley, T., Tilling, R., 2024. Estimating differential penetration of green (532 nm) laser light over sea ice with NASA's Airborne Topographic Mapper: observations and models. The Cryosphere 18, 2625–2652. https://doi.org/10.5194/tc-18-2625-2024.

113. Sun-Mack, S., Hu, Y., Lu, X., Chen, Y., Omar, A., 2025. Neural network-based snow depth retrieval from AMSR-2 brightness temperatures using ICESat-2 measurement as ground truth. Front. Remote Sensing 6, 1591276. https://doi.org/10.3389/frsen.2025.1591276.

114. Tilling, R. L., Ridout, A., and Shepherd, A., 2018. Estimating Arctic sea ice thickness and volume using CryoSat-2 radar altimeter data. Advances in Space Research 62, 1203–1225. https://doi.org/10.1016/j.asr.2017.10.051.

115. Tilling, R., Kurtz, N.T., Bagnardi, M., Petty, A.A., Kwok, R. 2020. Detection of melt ponds on Arctic summer sea ice from ICESat-2. Geophysical Research Letters 47, e2020GL090644.https://doi.org/10.1029/2020GL090644.

116. Urban, T. J., Schutz, B.E., 2005. ICESat sea level comparisons. Geophysical Research Letters 32, L23S10, https://10.1029/2005GL024306.

117. Urban, T. J., Schutz, B.E., Neuenschwander, A.L., 2008. A survey of ICESat coastal altimetry applications: Continental coast, open ccean island, and inland river. Terrestrial Atmospheric and Oceanic Sciences Journal 9, 1-19. https://10.3319/TAO.2008.19.1-2.1(SA).

118. van den Broeke, M., Box, J., Fettweis, X., Hanan, E, Noël, B., Tedesco, M., et al., 2017. Greenland Ice Sheet Surface Mass Loss: Recent Developments in Observation and Modeling. Current Climate Change Reports 3, 345–356. https://doi.org/10.1007/s40641-017-0084-8.

119. Walker, C.C., Becker, M.K., Fricker, H.A., 2021. A high resolution, three-dimensional view of the D-28 calving event from Amery Ice Shelf with ICESat-2 and satellite imagery. Geophysical Research Letters 48, e2020GL091200. https://doi.org/10.1029/2020GL091200.

120. Wang, G.Y., Ke, C.Q., Fan, Y.B., Shen, X.Y., Cai, Y., Nourani, V., 2024. Accelerated glacier mass loss in the mid-latitude Eurasia from 2019 to 2022 revealed by ICESat-2. Advances in Climate Change Research 15(5), 815-829. https://doi.org/10.1016/j.accre.2024.09.008.

https://doi.org/10.5194/egusphere-2026-288
Preprint. Discussion started: 10 February 2026

121. Wang, M., Oppelt, N., 2023. Estimating Early Summer Snow Depth on Sea Ice Using a Radiative Transfer Model and Optical Satellite Data. Remote Sensing 15, 5016. https://doi.org/10.3390/rs15205016.

122. Wang, S., Alexander, P., Wu, Q., Tedesco, M., 2021. Characterization of ice shelf fracture features using ICESat-2 – A case study over the Amery Ice Shelf. Remote Sensing of Environment 255, 112266. https://doi.org/10.1016/j.rse.2020.112266Get rights and content.

123. Webster, M.A., Holland, M., Wright, N.C., Hendricks, S., Hutter, N., Itkin, P., Light, B., Linhardt, F., et al., 2022. Spatiotemporal Evolution of Melt Ponds on Arctic Sea Ice: MOSAiC Observations and Model Results. Elementa: Science of the Anthropocene 10, 000072. https://doi.org/10.1525/elementa.2021.000072.

124. Wingham, D., Siegert, M., Shepherd, A., Muir, A.S., 2006. Rapid discharge connects Antarctic subglacial lakes. Nature 440, 1033–1036. https://doi.org/10.1038/nature04660.

125. Xiao, W., Hui, F., Cheng, X., Liang, Q., 2023. An automated algorithm to retrieve the location and depth of supraglacial lakes from ICESat-2 ATL03 data. Remote Sensing of Environment 298, 113730. https://doi.org/10.1016/j.rse.2023.113730.

126. Xie, T., Kong, R., Nurunnabi, A., Bai, S., Zhang, X., 2023. Machine-learning-method-based inversion of shallow bathymetric maps using ICESat-2 ATL03 data. IEEE J Sel Top. Appl. Earth Observations Remote Sensing 16, 3697-3714. https://doi.org/10.1109/JSTARS.2023.3260831.

127. Xu, Y., Li, H., Liu, B., Xie, H., Ozsoy-Cicek, B., 2021. Deriving Antarctic sea-ice thickness from satellite altimetry and estimating consistency for NASA's ICESat/ICESat-2 missions. Geophysical Research Letters 48, e2021GL093425. https://doi.org/10.1029/2021GL093425.

128. Yan, Z.N, Ji, Q., He, B., Chen, Y.Z, Wang, Y.Y., & Pang, X.P., 2024. A combined multi-source data and deep learning approach for retrieving snow depth on Antarctic Sea ice during the melting season. International Journal of Digital Earth, 17(1). https://doi.org/10.1080/17538947.2024.2376260.

129. Yang, B., Liang, S., Huang, H., Li, X., 2022. An elevation change dataset in Greenland ice sheet from 2003 to 2020 using satellite altimetry data. Big Earth Data 8(2), 231–248. https://doi.org/10.1080/20964471.2022.2116796.

130. Yang, R.Y., Zhong, Y.F., Su, Y., 2025. Multi-E2E: An end-to-end urban land-use mapping framework integrating high-resolution remote sensing images and multi-source geographical data Remote Sensing of Environment 330, 114966. https://doi.org/10.1016/j.rse.2025.114966

131. You, Q.L., Cai, Z.Y., Pepin, N., Chen, D.L., Ahrens, B., Jiang, Z.H., et al., 2021. Warming amplification over the Arctic Pole and Third Pole: Trends, mechanisms and consequences. Earth-Science Reviews 217, 103625. https://doi.org/10.1016/j.earscirev.2021.103625.

132. Yu, J., Nie, S., Liu, W., Zhu, X., Sun, Z., Li, J., et al., 2024. Mapping global mangrove canopy height by integrating ice, cloud, and land elevation Satellite-2 photon-counting LiDAR data with multi-source images. Science of the Total Environment 939, 173487. https://doi.org/10.1016/j.scitotenv.2024.173487.

133. Zeng, X., Broxton, P., Dawson, N., 2018. Snowpack Change from 1982-2016 over Conterminous United States. Geophysical Research Letters 15, 12940–12947. https://doi.org/10.1029/2018GL079621.

134. Zhang, B., Wang, Z., Yang, Q., Liu, J., An, J., Li, F., et al., 2020. Elevation Changes of the Antarctic Ice Sheet from Joint Envisat and CryoSat-2 Radar Altimetry. Remote Sening 12, 3746. https://doi.org/10.3390/rs12223746.

135. Zhang, D.F., Chen, Y.F., Le, Y., Dong, Y.S., Dai, G.M., Wang, L.Z., 2022. Refraction and coordinate correction with the JONSWAP model for ICESat-2 bathymetry. ISPRS Jouunal of Photogrammetry and Remote Sensing 186, 285-300. https://doi.org/10.1016/j.isprsjprs.2022.02.020.

136. Zhang, F.Y, Lei, R.B, Zhai, M.X, Pang, X.P, Li, N., 2023. The impacts of anomalies in atmospheric circulations on Arctic sea ice outflow and sea ice conditions in the Barents and Greenland seas: case study in 2020. The Cryosphere 17, 4609–4628. https://doi.org/10.5194/tc-17-4609-2023.

137. Zhang, Q., Huai, B., van Den Broeke, M.R.,Cappelen, J., Ding, M.H., Wang, Y.T., 2022b. Temporal and Spatial Variability in Contemporary Greenland Warming (1958–2020). Journal of Climate 35(9): 2755-2767. https://doi.org/10.1175/JCLI-D-21-0313.1.

https://doi.org/10.5194/egusphere-2026-288
Preprint. Discussion started: 10 February 2026

138. Zhang, T., Price, S., Ju, L., Leng, W., Brondex, J., Durand, G., et al., 2017. A comparison of two Stokes ice sheet models applied to the Marine Ice Sheet Model Intercomparison Project for plan view models (MISMIP3d). The Cryosphere 11, 179–190. https://doi.org/10.5194/tc-11-179-201.

139. Zhang, X., Ma, Y., Zhang, F., Li, Z., Zhang, J., 2025. Multi-Model Synergistic Satellite-Derived Bathymetry Fusion Approach Based on Mamba Coral Reef Habitat Classification. Remote Sensing 17, 2134. https://doi.org/10.3390/rs17132134.

140. Zhao, X., Huo, R., Chen, Y.Z, Ma, Y., Ji, Q., Pang, X.P., 2024. Route Planning in the Arctic Ice Region Assisted by ICESat-2 Elevation Information. Geomatics and Information Science of Wuhan University 49(9) 1610-1620. In Chinese with English abstract.

141. Zhou, L., Xu, S., Liu, J., Wang, B., 2018. On the retrieval of sea ice thickness and snow depth using concurrent laser altimetry and L-band remote sensing data. The Cryosphere 12, 993–1012. https://doi.org/10.5194/tc-12-993-2018.

142. Zhu, X., Wang, C., Nie, S., Pan, F., Xi, X., Hu, Z., 2020. Mapping forest height using photon-counting LiDAR data and Landsat 8 OLI data: a case study in Virginia and North Carolina, USA. Ecological Indicators 114, 106287. https://doi.org/10.1016/j.ecolind.2020.106287.

143. Niehaus, H., Spreen, G., Istomina, L., and Nicolaus, M., 2025. Regional and seasonal evolution of melt ponds on Arctic sea ice. The Cryosphere, 19, 3915–3938, https://doi.org/10.5194/tc-19-3915-2025.

144. Magruder, L., Neumann, T., Kurtz, N., 2021. ICESat-2 early mission synopsis and observatory performance. Earth and Space Science, 8, e2020EA001555. https://doi.org/10.1029/2020EA001555.